Journal of Computational Physics 523 (2025) 113605

Contents lists available at ScienceDirect

Journal of Computational Physics

journal homepage: www.elsevier.com/locate/jcp

A stabilized parametric finite element method for surface diffusion with an arbitrary surface energy

Yulin Zhang [a], Yifei Li [b,*], Wenjun Ying [a]

[a] School of Mathematical Sciences, MOE-LSC and Institute of Natural Sciences, Shanghai Jiao Tong University, Shanghai 200240, PR China
[b] Department of Mathematics, National University of Singapore, 119076, Singapore

ARTICLE INFO

Keywords:
Geometric flows
Parametric finite element method
Anisotropy surface energy
Structure-preserving
Area conservation
Energy-stable

ABSTRACT

We proposed a structure-preserving stabilized parametric finite element method (SPFEM) for the evolution of closed curves under anisotropic surface diffusion with an arbitrary surface energy $\hat{\gamma}(\theta)$. By introducing a non-negative stabilizing function $k(\theta)$ depending on $\hat{\gamma}(\theta)$, we obtained a novel stabilized conservative weak formulation for the anisotropic surface diffusion. A SPFEM is presented for the discretization of this weak formulation. We construct a comprehensive framework to analyze and prove the unconditional energy stability of the SPFEM under a very mild condition on $\hat{\gamma}(\theta)$, including the critical case where $3\hat{\gamma}(\theta^*) = \hat{\gamma}(\theta^* - \pi)$. This method can be applied to simulate solid-state dewetting of thin films with arbitrary surface energies, which are characterized by anisotropic surface diffusion and contact line migration. Extensive numerical results are reported to demonstrate the efficiency, accuracy and structure-preserving properties of the proposed SPFEM with anisotropic surface energies $\hat{\gamma}(\theta)$ arising from different applications.

1. Introduction

Surface diffusion is a widespread process involving the movement of atoms, molecules and atomic clusters at solid material interfaces [39]. Due to different surface lattice orientation, an anisotropic evolution process is generated for a solid material, which is called *anisotropic surface diffusion* in the literature. Surface diffusion with an anisotropic surface energy plays an important role as a crucial mechanism and/or kinetics in various fields such as epitaxial growth [23,28], surface phase formation [52], heterogeneous catalysis [40], and other pertinent fields within surface and materials science [13,42,43]. In fact, broader and consequential applications of surface diffusion have been discovered in materials science and solid-state physics, notably in areas such as the crystal growth of nanomaterials [25,26] and solid-state dewetting [6,29,31,33,44,48,49,52].

As shown in Fig. 1, let $\Gamma := \Gamma(t)$ be a closed curve in two dimensions (2D) associated with a given anisotropic surface energy $\hat{\gamma}(\theta) > 0$, where $\theta \in 2\pi\mathbb{T} := \mathbb{R}/2\pi\mathbb{Z}$ represents the angle between the vertical axis and unit outward normal vector $\boldsymbol{n} = \boldsymbol{n}(\theta) := (-\sin\theta, \cos\theta)^T$. It should be noted that the anisotropy can also be viewed as a function $\gamma(\boldsymbol{n})$ of the normal vector $\boldsymbol{n}$ [32,33,46]. While $\gamma(\boldsymbol{n}) = \gamma(-\sin\theta, \cos\theta)$ is equivalent to $\hat{\gamma}(\theta)$ by the one-to-one correspondence $\boldsymbol{n}(\theta) = (-\sin\theta, \cos\theta)^T$, the $\hat{\gamma}(\theta)$ formulation is often more convenient and straightforward in 2D.

Suppose Γ is represented by $\boldsymbol{X} := \boldsymbol{X}(s,t) = (x(s,t), y(s,t))^T$, where s denotes the arc-length parameter, and t represents the time. The motion of Γ under anisotropic surface diffusion is governed by the following geometric flow [18,38]:

* Corresponding author.
E-mail addresses: yulin.zhang@sjtu.edu.cn (Y. Zhang), liyifei@nus.edu.sg (Y. Li), wying@sjtu.edu.cn (W. Ying).

https://doi.org/10.1016/j.jcp.2024.113605
Received 2 April 2024; Received in revised form 19 September 2024; Accepted 19 November 2024

Available online 22 November 2024

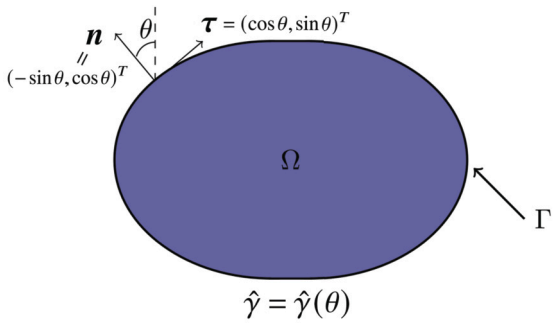

Fig. 1. An illustration of a closed curve under anisotropic surface diffusion with an anisotropic surface energy $\hat{\gamma}(\theta)$, while θ is the angle between the y-axis and the unit outward normal vector $\boldsymbol{n} = \boldsymbol{n}(\theta) := (-\sin\theta, \cos\theta)^T$. $\boldsymbol{\tau} = \boldsymbol{\tau}(\theta) := (\cos\theta, \sin\theta)^T$ represents the unit tangent vector.

$$\partial_t \boldsymbol{X} = \partial_{ss}\mu\boldsymbol{n}, \tag{1.1}$$

where μ is the weighted curvature (or chemical potential) defined as

$$\mu := [\hat{\gamma}(\theta) + \hat{\gamma}''(\theta)]\kappa \tag{1.2}$$

with $\kappa := -(\partial_{ss}\boldsymbol{X}) \cdot \boldsymbol{n}$ being the curvature.

The anisotropic surface diffusion (1.1) is a fourth-order and highly nonlinear geometric flow, which possesses two major geometric properties, i.e., the area conservation and the energy dissipation. Let $A_c(t)$ be the area of the region $\Omega(t)$ enclosed by $\Gamma(t)$, and $W_c(t)$ be the total surface free energy, which are defined as

$$A_c(t) := \int_{\Omega(t)} 1\,\mathrm{d}x\mathrm{d}y = \int_{\Gamma(t)} y(s,t)\partial_s x(s,t)\,\mathrm{d}s, \qquad W_c(t) := \int_{\Gamma(t)} \hat{\gamma}(\theta)\,\mathrm{d}s. \tag{1.3}$$

One can prove that [4,6,13]

$$\frac{\mathrm{d}}{\mathrm{d}t}A_c(t) = \int_{\Gamma(t)} \partial_{ss}\mu\,\mathrm{d}s = 0, \qquad \frac{\mathrm{d}}{\mathrm{d}t}W_c(t) = \int_{\Gamma(t)} \mu\,\partial_{ss}\mu\,\mathrm{d}s = -\int_{\Gamma(t)} |\partial_s\mu|^2\,\mathrm{d}s \le 0, \tag{1.4}$$

which immediately implies the anisotropic surface diffusion (1.1)-(1.2) satisfies the area conservation and energy dissipation, i.e.,

$$A_c(t) \equiv A_c(0), \qquad W_c(t) \le W_c(t_1) \le W_c(0), \qquad \forall t \ge t_1 \ge 0. \tag{1.5}$$

When $\hat{\gamma}(\theta) \equiv 1, \forall\theta \in 2\pi\mathbb{T}$, the weighted curvature μ reduces to κ, and it is referred to as *isotropic* surface energy. If $\hat{\gamma}(\theta)$ is not a constant function and $\hat{\gamma}(\theta) + \hat{\gamma}''(\theta) > 0$ for all $\theta \in 2\pi\mathbb{T}$, we classify the surface energy as *weakly anisotropic*, otherwise, it is termed *strongly anisotropic*. Typical anisotropic surface energies $\hat{\gamma}(\theta)$ which are widely employed in materials science include:

1. the m-fold anisotropic surface energy [4]

$$\hat{\gamma}(\theta) = 1 + \beta\cos m(\theta - \theta_0), \qquad \theta \in 2\pi\mathbb{T}, \tag{1.6}$$

   where $m = 2, 3, 4, 6, |\beta| < 1$ are dimensionless strength constants, $\theta_0 \in 2\pi\mathbb{T}$ is a constant. Note that $\hat{\gamma}(\theta)$ is weakly anisotropic when $|\beta| < \frac{1}{m^2-1}$, and strongly anisotropic otherwise.
2. the ellipsoidal anisotropic surface energy [47]

$$\hat{\gamma}(\theta) = \sqrt{a + b\cos^2\theta}, \qquad \theta \in 2\pi\mathbb{T}, \tag{1.7}$$

   where a, b are two dimensionless constants satisfying $a > 0$ and $a + b > 0$.
3. the Riemannian-like metric (also called BGN) anisotropic surface energy [14,16]

$$\hat{\gamma}(\theta) = \sum_{l=1}^{L} \sqrt{\boldsymbol{n}(\theta)^T G_l \boldsymbol{n}(\theta)}, \qquad \boldsymbol{n} = (-\sin\theta, \cos\theta)^T, \qquad \theta \in 2\pi\mathbb{T}, \tag{1.8}$$

   where $L \ge 1$, $G_l \in \mathbb{R}^{2\times 2}$ positive definite $\forall 1 \le l \le L$. When $L = 1, G_1 = \mathrm{diag}(a, a + b)$ in (1.8), the Riemannian-like metric anisotropy (1.8) collapses to the ellipsoidal anisotropic surface energy (1.7).
4. the piecewise anisotropic surface energy [20]

$$\hat{\gamma}(\theta) = \sqrt{\left(\frac{5}{2} + \frac{3}{2}\mathrm{sgn}(n_1)\right) n_1^2 + n_2^2}, \tag{1.9}$$

   with $\boldsymbol{n} = (n_1, n_2)^T := (-\sin\theta, \cos\theta)^T$, $\theta \in 2\pi\mathbb{T}$.

Many numerical methods have been proposed for simulating the evolution of curves under surface diffusion, including the phase-field method [22,24,29,45], the discontinuous Galerkin method [51], the marker particle method [21,50] and the parametric finite element method (PFEM) [1,12,15,17]. Among these methods, the energy-stable PFEM (ES-PFEM) by Barrett, Garcke, and Nürnberg [12], also referred to as BGN's method, achieves the best performance in terms of mesh quality and unconditional energy-stability in the isotropic case. The ES-PFEM has been further extended to other geometric flows, such as the solid-state deweting problem [4,30,49], demonstrating its adaptability and robustness. Furthermore, Bao and Zhao have recently developed a structure-preserving PFEM (SP-PFEM) [2,3,11], which can preserve the enclosed mass at the fully-discretized level while also maintaining the unconditional energy stability. Extending these PFEMs to anisotropic surface diffusion is a major focus of recent research in surface diffusion. While BGN successfully adapted their methods to a specific Riemannian metric form [14,16], designing a SP-PFEM for anisotropic surface diffusion with arbitrary anisotropies remains challenging.

Lately, based on the $\hat{\gamma}(\theta)$ formulation, Li and Bao introduced a surface energy matrix $G(\theta)$ and extend the ES-PFEM from the isotropic cases to the anisotropic cases [36]. Due to the absence of a stabilizing term, their method requires a certain restrictive condition to ensure the energy stability. Subsequently, Bao, Jiang, and Li incorporated a stabilizing function within the $\gamma(\boldsymbol{n})$ formulation. They constructed a symmetric surface energy matrix $\boldsymbol{Z}_k(\boldsymbol{n})$ and proposed a symmetrized SP-PFEM for the anisotropic surface diffusion in [5,8]. Shortly afterward, it was extended to evolutions of open curves in solid-state dewetting [35]. The symmetrized SP-PFEM with the stabilizing function works effectively for symmetric surface energy distributions (i.e., $\gamma(\boldsymbol{n}) = \gamma(-\boldsymbol{n})$) to maintain the geometric properties. However, there are different anisotropic surface energies $\hat{\gamma}(\theta)$ which are not symmetrically distributed or do not satisfy the specific condition, such as the 3-fold anisotropic surface energy (1.6) [4,49]. Very recently, based on the $\gamma(\boldsymbol{n})$ formulation, Bao and Li introduced a novel surface energy matrix and established a comprehensive analytical framework to demonstrate the unconditional energy stability of the proposed SP-PFEM [7,9]. Based on this framework, they successfully reduced the requirement for the anisotropy to $3\gamma(\boldsymbol{n}) > \gamma(-\boldsymbol{n})$, $\forall \boldsymbol{n} \in \mathbb{S}^1$.

However, the critical situation $3\gamma(\boldsymbol{n}^*) = \gamma(-\boldsymbol{n}^*)$, $\boldsymbol{n}^* \in \mathbb{S}^1$ was not addressed in their analytical framework. It is natural to consider the derivative for this critical case. However, analyzing the gradient of $\gamma(\boldsymbol{n})$ is challenging since it is defined on the unit sphere $\mathbb{S}^1$. In contrast, the $\hat{\gamma}(\theta)$ formulation, defined on $2\pi\mathbb{T}$, possesses a simpler derivative and thus allows for a better analysis of the critical situation $3\hat{\gamma}(\theta^*) = \hat{\gamma}(\theta^* - \pi)$, $\theta^* \in 2\pi\mathbb{T}$. Based on this key insight, we are able to provide an elaborate investigation of the critical situation, extending the previously analysis framework to $3\hat{\gamma}(\theta^*) = \hat{\gamma}(\theta^* - \pi)$.

The main objective of this paper is to propose a structure-preserving stabilized parametric finite element method (SPFEM) for simulating surface diffusion (1.1) with the surface energy $\hat{\gamma}(\theta)$ under very mild conditions as

(i) $3\hat{\gamma}(\theta) \geq \hat{\gamma}(\theta - \pi), \qquad \forall \theta \in 2\pi\mathbb{T},$
(ii) $\hat{\gamma}'(\theta^*) = 0$, when $3\hat{\gamma}(\theta^*) = \hat{\gamma}(\theta^* - \pi), \qquad \theta^* \in 2\pi\mathbb{T}.$

Compared to the $\gamma(\boldsymbol{n})$ formulation, the $\hat{\gamma}(\theta)$ formulation has the following advantages:

(i) it is more intuitive and has a simpler form in practical applications;
(ii) it enables a reduction in the regularity requirement for the anisotropy from C^2 to globally C^1 and piecewise C^2;
(iii) it allows for a more convenient discussion of critical situations as $3\hat{\gamma}(\theta^*) = \hat{\gamma}(\theta^* - \pi)$ for some $\theta^* \in 2\pi\mathbb{T}$ in 2D.

The remainder of this paper is organized as follows: In section 2, we introduce a stabilized surface energy matrix $\hat{\boldsymbol{G}}_k(\theta)$ and propose a new conservative formulation for anisotropic surface diffusion. In section 3, we present a novel weak formulation based on the conservative form, introduce its spatial semi-discretization, and propose a full discretization by SPFEM. In section 4, we analyze the structure-preserving properties of the proposed scheme, i.e., area conservation and unconditional energy stability, and develop a comprehensive framework for energy stability. It starts from defining a minimal stabilizing function $k_0(\theta)$, then we obtain the main result through a local energy estimate under the assumption that $k_0(\theta)$ is well-defined. The existence of $k_0(\theta)$ is further demonstrated in section 5. In section 6, we extend the SPFEM for simulating solid-state dewetting of thin films under anisotropic surface diffusion and contact line migration. Extensive numerical results are provided in section 7 to demonstrate the efficiency, accuracy and structure-preserving properties of the proposed SPFEM. Finally, we conclude in section 8.

2. A conservative formulation

In this section, we propose a novel formulation with stabilization for (1.1) and derive a conservative form by introducing a stabilized surface energy matrix.

Applying the geometric identity $\kappa\boldsymbol{n} = -\partial_{ss}\boldsymbol{X}$ [37], the anisotropic surface diffusion equations (1.1)-(1.2) can be reformulated into

$$\boldsymbol{n} \cdot \partial_t \boldsymbol{X} - \partial_{ss}\mu = 0, \qquad 0 < s < L(t), \qquad t > 0, \tag{2.1a}$$

$$\mu\boldsymbol{n} + \left[\hat{\gamma}(\theta) + \hat{\gamma}''(\theta)\right]\partial_{ss}\boldsymbol{X} = \boldsymbol{0}, \tag{2.1b}$$

where $L(t) = \int_{\Gamma(t)} \mathrm{d}s$ is the length of $\Gamma(t)$.

For a vector $\boldsymbol{v} = (v_1, v_2)^T \in \mathbb{R}^2$, we denote $\boldsymbol{v}^\perp \in \mathbb{R}^2$ as its perpendicular vector which is the clockwise rotation of $\boldsymbol{v}$ by $\frac{\pi}{2}$, i.e.

$$\boldsymbol{v}^\perp := (v_2, -v_1)^T = -\boldsymbol{J}\boldsymbol{v}, \qquad \text{with} \quad \boldsymbol{J} = \begin{pmatrix} 0 & -1 \\ 1 & 0 \end{pmatrix}. \tag{2.2}$$

Then the tangent vector $\boldsymbol{\tau} := \partial_s \boldsymbol{X}$, and unit normal vector $\boldsymbol{n}$ can be written as $\boldsymbol{n} = -\boldsymbol{\tau}^\perp$. And the tangent vector can also be given by $\boldsymbol{\tau} = \boldsymbol{n}^\perp$.

Theorem 2.1. *For the weighted curvature μ given in (1.2), the following identity holds:*

$$\mu \boldsymbol{n} = -\partial_s \left(\hat{\boldsymbol{G}}_k(\theta) \partial_s \boldsymbol{X} \right), \tag{2.3}$$

with

$$\hat{\boldsymbol{G}}_k(\theta) = \begin{pmatrix} \hat{\gamma}(\theta) & -\hat{\gamma}'(\theta) \\ \hat{\gamma}'(\theta) & \hat{\gamma}(\theta) \end{pmatrix} + k(\theta) \begin{pmatrix} \sin^2\theta & -\cos\theta\sin\theta \\ -\cos\theta\sin\theta & \cos^2\theta \end{pmatrix}, \qquad \forall \theta \in 2\pi\mathbb{T}, \tag{2.4}$$

$k(\theta) : 2\pi\mathbb{T} \to \mathbb{R}_{\geq 0}$ is a non-negative stabilizing function.

Proof. Noticing

$$\boldsymbol{n} = -\partial_s \boldsymbol{X}^\perp = (-\partial_s y, \partial_s x)^T, \qquad \partial_s x = \cos\theta, \qquad \partial_s y = \sin\theta, \tag{2.5}$$

therefore

$$\partial_{ss} x = -\sin\theta \partial_s \theta, \qquad \partial_{ss} y = \cos\theta \partial_s \theta, \tag{2.6}$$

which implies that

$$\kappa = -(\partial_{ss}\boldsymbol{X}) \cdot \boldsymbol{n} = \partial_{ss} x \partial_s y - \partial_{ss} y \partial_s x = -(\sin^2\theta + \cos^2\theta)\partial_s\theta = -\partial_s\theta. \tag{2.7}$$

By the geometric identity $\kappa \boldsymbol{n} = -\partial_{ss}\boldsymbol{X}$ and $\partial_s \boldsymbol{X} = \tau = \boldsymbol{n}^\perp$, we obtain

$$\kappa \partial_s \boldsymbol{X} = \kappa \boldsymbol{n}^\perp = -\partial_{ss}\boldsymbol{X}^\perp, \qquad \kappa \partial_s \boldsymbol{X}^\perp = -\kappa \boldsymbol{n} = \partial_{ss}\boldsymbol{X}. \tag{2.8}$$

Then by (2.7) and (2.8),

$$\begin{aligned} \partial_s \left(\hat{\gamma}(\theta) \partial_s \boldsymbol{X} \right) &= \hat{\gamma}'(\theta) \partial_s\theta \partial_s \boldsymbol{X} + \hat{\gamma}(\theta) \partial_{ss}\boldsymbol{X} \\ &= -\kappa \hat{\gamma}'(\theta) \partial_s \boldsymbol{X} + \hat{\gamma}(\theta) \partial_{ss}\boldsymbol{X} \\ &= \hat{\gamma}''(\theta) \partial_{ss}\boldsymbol{X}^\perp + \hat{\gamma}(\theta) \partial_{ss}\boldsymbol{X}, \end{aligned} \tag{2.9}$$

and

$$\begin{aligned} \partial_s \left(\hat{\gamma}'(\theta) \partial_s \boldsymbol{X}^\perp \right) &= \hat{\gamma}''(\theta) \partial_s\theta \partial_s \boldsymbol{X}^\perp + \hat{\gamma}'(\theta) \partial_{ss}\boldsymbol{X}^\perp \\ &= -\kappa \hat{\gamma}''(\theta) \partial_s \boldsymbol{X}^\perp + \hat{\gamma}'(\theta) \partial_{ss}\boldsymbol{X}^\perp \\ &= -\hat{\gamma}''(\theta) \partial_{ss}\boldsymbol{X} + \hat{\gamma}'(\theta) \partial_{ss}\boldsymbol{X}^\perp. \end{aligned} \tag{2.10}$$

Note that $\boldsymbol{n}^T \partial_s \boldsymbol{X} = \boldsymbol{n} \cdot \boldsymbol{\tau} \equiv 0$, thus $\partial_s \left(k(\theta) \boldsymbol{n}\boldsymbol{n}^T \partial_s \boldsymbol{X} \right)$ vanishes. Combining (2.1b), (2.9) and (2.10), we have

$$\begin{aligned} \mu \boldsymbol{n} &= -[\hat{\gamma}(\theta) + \hat{\gamma}''(\theta)] \partial_{ss}\boldsymbol{X} - \partial_s \left(k(\theta) \boldsymbol{n}\boldsymbol{n}^T \partial_s \boldsymbol{X} \right) \\ &= -\partial_s \left(\hat{\gamma}(\theta) \partial_s \boldsymbol{X} \right) + \partial_s \left(\hat{\gamma}'(\theta) \partial_s \boldsymbol{X}^\perp \right) - \partial_s \left(k(\theta) \boldsymbol{n}\boldsymbol{n}^T \partial_s \boldsymbol{X} \right) \\ &= -\partial_s \left(\hat{\gamma}(\theta) \partial_s \boldsymbol{X} - \hat{\gamma}'(\theta) \partial_s \boldsymbol{X}^\perp + k(\theta) \boldsymbol{n}\boldsymbol{n}^T \partial_s \boldsymbol{X} \right). \end{aligned} \tag{2.11}$$

On the other hand, by (2.5), we have

$$\begin{pmatrix} \sin^2\theta & -\sin\theta\cos\theta \\ -\sin\theta\cos\theta & \cos^2\theta \end{pmatrix} = \begin{pmatrix} -\sin\theta \\ \cos\theta \end{pmatrix} (-\sin\theta, \cos\theta) = \boldsymbol{n}\boldsymbol{n}^T, \tag{2.12}$$

consequently

$$\begin{aligned} \hat{\boldsymbol{G}}_k(\theta) \partial_s \boldsymbol{X} &= \left[\begin{pmatrix} \hat{\gamma}(\theta) & -\hat{\gamma}'(\theta) \\ \hat{\gamma}'(\theta) & \hat{\gamma}(\theta) \end{pmatrix} + k(\theta) \begin{pmatrix} \sin^2\theta & -\sin\theta\cos\theta \\ -\sin\theta\cos\theta & \cos^2\theta \end{pmatrix} \right] \partial_s \boldsymbol{X} \\ &= \left[\hat{\gamma}(\theta) I_2 + \hat{\gamma}'(\theta) J + k(\theta) \boldsymbol{n}\boldsymbol{n}^T \right] \partial_s \boldsymbol{X} \\ &= \hat{\gamma}(\theta) \partial_s \boldsymbol{X} - \hat{\gamma}'(\theta) \partial_s \boldsymbol{X}^\perp + k(\theta) \boldsymbol{n}\boldsymbol{n}^T \partial_s \boldsymbol{X}, \end{aligned} \tag{2.13}$$

where I_2 is the 2×2 identity matrix. Substituting (2.13) into (2.11), the desired equality (2.3) is obtained. □

Applying (2.3), the governing geometric PDE (2.1) for anisotropic surface diffusion can be reformulated as the following *conservative form*

$$\boldsymbol{n}\cdot\partial_t\boldsymbol{X}-\partial_{ss}\mu=0, \tag{2.14a}$$

$$\mu\boldsymbol{n}+\partial_s\left(\hat{\boldsymbol{G}}_k(\theta)\partial_s\boldsymbol{X}\right)=0. \tag{2.14b}$$

Remark 2.1. For the isotropic case, the curvature vector $\kappa\boldsymbol{n}=-\partial_{ss}\boldsymbol{X}=-\partial_s\left(I_2\partial_s\boldsymbol{X}\right)$ which inspired us to construct a proper stabilized conservative form as $\mu\boldsymbol{n}=-\partial_s\left(\hat{\boldsymbol{G}}_k(\theta)\partial_s\boldsymbol{X}\right)$ for the anisotropic case. The construction of the stabilization term is based on the following two ideas: i) the stabilization term should make no contribution at the continuous level, i.e. the tangent vector $\partial_s\boldsymbol{X}$ lies in the kernel of the stabilization term; ii) the stabilization term should be positive definite which brings numerous numerical advantages. Therefore, the stabilization term is formulated as $k(\theta)\boldsymbol{n}\boldsymbol{n}^T=k(\theta)\begin{pmatrix}\sin^2\theta & -\cos\theta\sin\theta\\ -\cos\theta\sin\theta & \cos^2\theta\end{pmatrix}$.

Remark 2.2. If we take the stabilizing function $k(\theta)\equiv 0$ in (2.4), then $\hat{\boldsymbol{G}}_k(\theta)=\begin{pmatrix}\hat\gamma(\theta) & -\hat\gamma'(\theta)\\ \hat\gamma'(\theta) & \hat\gamma(\theta)\end{pmatrix}$ collapses to the surface energy matrix $G(\theta)$ proposed in [36]. Moreover, with the adoption of the $\gamma(\boldsymbol{n})$ formulation, we can define the corresponding stabilizing function $k(\boldsymbol{n}):=k(\boldsymbol{n}(\theta))=k(\theta)$ by the one-to-one correspondence $\boldsymbol{n}=\boldsymbol{n}(\theta)=(-\sin\theta,\cos\theta)^T$, and the stabilization term is simplified to $k(\boldsymbol{n})\boldsymbol{n}\boldsymbol{n}^T$. Consequently, $\hat{\boldsymbol{G}}_k(\theta)$ is transformed into the surface energy matrix $\boldsymbol{G}_k(\boldsymbol{n})$ in [7].

Remark 2.3. At the continuous level, $k(\theta)$ makes no contribution, as $\boldsymbol{n}^T\partial_s\boldsymbol{X}=0$. Thus, the conservative form (2.14) and the original form (2.1) are equivalent. At the discrete level, however, $k(\theta)$ serves as a stabilizing term, which relaxes the energy stability conditions for the anisotropy $\hat\gamma(\theta)$. For example, surface matrix $G(\theta)$ in [36] (absent the stabilizing term) only guarantees energy stability for specific cases of weakly anisotropic surface energy. In contrast, with this stabilizing term, this formulation can be applied to more general anisotropies, see (3.36)

3. A SPFEM for anisotropic surface diffusion

In this section, we first develop a novel weak formulation based on the conservative form (2.14) and present the spatial semi-discretization of this weak formulation. After that, a structure-preserving SPFEM is proposed by adapting the implicit-explicit Euler method in time, which preserves area conservation and energy dissipation at the discrete level.

3.1. Weak formulation

In order to derive a weak formulation of equation (2.14), we introduce a time-independent variable ρ which parameterizes $\Gamma(t)$ over a fixed domain $\rho\in\mathbb{I}=[0,1]$ as

$$\Gamma(t):=\boldsymbol{X}(\rho,t)=(x(\rho,t),y(\rho,t))^T:\mathbb{I}\times\mathbb{R}^+\to\mathbb{R}^2. \tag{3.1}$$

The arc-length parameter s can thus be computed by $s=\int_0^\rho|\partial_\rho\boldsymbol{X}(q,t)|\,\mathrm{d}q$. (We do not distinguish $\boldsymbol{X}(\rho,t)$ and $\boldsymbol{X}(s,t)$ if there's no misunderstanding.)

Introduce the following functional space with respect to the evolution curve $\Gamma(t)$ as

$$L^2(\mathbb{I}):=\left\{u:\mathbb{I}\to\mathbb{R}\,|\int_{\Gamma(t)}|u(s)|^2\,\mathrm{d}s=\int_{\mathbb{I}}|u(s(\rho,t))|^2\partial_\rho s\,\mathrm{d}s<+\infty\right\}, \tag{3.2}$$

equipped with the L^2-inner product

$$\left(u,v\right)_{\Gamma(t)}:=\int_{\Gamma(t)}u(s)v(s)\,\mathrm{d}s=\int_{\Gamma(t)}u(s(\rho,t))v(s(\rho,t))\partial_\rho s\,\mathrm{d}\rho, \tag{3.3}$$

for any scalar (or vector) functions. The Sobolev spaces are defined as

$$H^1(\mathbb{I}):=\left\{u:\mathbb{I}\to\mathbb{R}\,|\,u\in L^2(\mathbb{I}),\text{ and }\partial_\rho u\in L^2(\mathbb{I})\right\}, \tag{3.4a}$$

$$H^1_p(\mathbb{I}):=\left\{u\in H^1(\mathbb{I})\,|\,u(0)=u(1)\right\}. \tag{3.4b}$$

Extensions of above definitions to the functions in $[L^2(\mathbb{I})]^2,[H^1(\mathbb{I})]^2$ and $[H^1_p(\mathbb{I})]^2$ are straightforward.

By multiplying the equation (2.14a) by a test function $\varphi\in H^1_p(\mathbb{I})$, integrating over $\Gamma(t)$, and applying integration by parts, we obtain

$$\left(\boldsymbol{n}\cdot\partial_t\boldsymbol{X},\varphi\right)_{\Gamma(t)}+\left(\partial_s\mu,\partial_s\varphi\right)_{\Gamma(t)}=0. \tag{3.5}$$

Similarly, by taking the dot product of equation (2.14b) with a test function $\boldsymbol{\omega} = (\omega_1, \omega_2)^T \in [H_p^1(\mathbb{I})]^2$ and integrating by parts, we have

$$\begin{aligned} 0 &= \left(\mu \boldsymbol{n} + \partial_s \left(\hat{\boldsymbol{G}}_k(\theta)\partial_s \boldsymbol{X}\right), \boldsymbol{\omega}\right)_{\Gamma(t)} \\ &= \left(\mu \boldsymbol{n}, \boldsymbol{\omega}\right)_{\Gamma(t)} + \left(\partial_s(\hat{\boldsymbol{G}}_k(\theta)\partial_s \boldsymbol{X}), \boldsymbol{\omega}\right)_{\Gamma(t)} \\ &= \left(\mu \boldsymbol{n}, \boldsymbol{\omega}\right)_{\Gamma(t)} - \left(\hat{\boldsymbol{G}}_k(\theta)\partial_s \boldsymbol{X}, \partial_s \boldsymbol{\omega}\right)_{\Gamma(t)} \end{aligned} \tag{3.6}$$

Combining (3.5) and (3.6), we propose a new weak formulation for (2.14) as follows: Given an initial closed curve $\Gamma(0) := \boldsymbol{X}(\cdot, 0) = \boldsymbol{X}_0 \in [H_p^1(\mathbb{I})]^2$, find the solution $(\boldsymbol{X}(\cdot, t) = (x(\cdot, t), y(\cdot, t))^T, \mu(\cdot, t)) \in [H_p^1(\mathbb{I})]^2 \times H_p^1(\mathbb{I})$, such that:

$$\left(\boldsymbol{n} \cdot \partial_t \boldsymbol{X}, \varphi\right)_{\Gamma(t)} + \left(\partial_s \mu, \partial_s \varphi\right)_{\Gamma(t)} = 0, \qquad \forall \varphi \in H_p^1(\mathbb{I}), \tag{3.7a}$$

$$\left(\mu \boldsymbol{n}, \boldsymbol{\omega}\right)_{\Gamma(t)} - \left(\hat{\boldsymbol{G}}_k(\theta)\partial_s \boldsymbol{X}, \partial_s \boldsymbol{\omega}\right)_{\Gamma(t)} = 0, \qquad \forall \boldsymbol{\omega} \in [H_p^1(\mathbb{I})]^2. \tag{3.7b}$$

It can be demonstrated that the weak formulation (3.7) maintains two geometric properties, namely, area conservation and energy dissipation.

Proposition 3.1 *(Area conservation and energy dissipation). Suppose $\Gamma(t)$ is given by the solution $(\boldsymbol{X}(\cdot, t), \mu(\cdot, t))$ of the weak formulation (3.7), denote $A_c(t)$ as the enclosed area and $W_c(t)$ as the total energy of the closed evolving curve $\Gamma(t)$, respectively, which are formally given by*

$$A_c(t) := \int_{\Gamma(t)} y(s,t)\partial_s x(s,t)\,\mathrm{d}s, \qquad W_c(t) := \int_{\Gamma(t)} \hat{\gamma}(\theta)\,\mathrm{d}s. \tag{3.8}$$

Then we have

$$A_c(t) \equiv A_c(0), \qquad W_c(t) \le W_c(t_1) \le W_c(0), \qquad \forall t \ge t_1 \ge 0. \tag{3.9}$$

More precisely,

$$\frac{\mathrm{d}}{\mathrm{d}t} A_c(t) = 0, \qquad \frac{\mathrm{d}}{\mathrm{d}t} W_c(t) = -\int_{\Gamma(t)} |\partial_s \mu|^2\,\mathrm{d}s \le 0, \qquad t \ge 0. \tag{3.10}$$

To prove the above theorem, we first introduce the following transport lemma:

Lemma 3.1. *Suppose $\Gamma(t)$ is a two-dimensional piecewise C^1 curve parameterized by $\boldsymbol{X}(\rho, t)$, $f : \Gamma(t) \times \mathbb{R}^+ \to \mathbb{R}$ is a differentiable function, then*

$$\frac{\mathrm{d}}{\mathrm{d}t} \int_{\Gamma(t)} f\,\mathrm{d}s = \int_{\Gamma(t)} \partial_t f + f\partial_s(\partial_t \boldsymbol{X}) \cdot \partial_s \boldsymbol{X}\,\mathrm{d}s. \tag{3.11}$$

Proof. Since $|\partial_\rho \boldsymbol{X}| = \sqrt{(\partial_\rho x)^2 + (\partial_\rho y)^2}$, then

$$\begin{aligned} \partial_t |\partial_\rho \boldsymbol{X}| &= \frac{\partial_\rho x \partial_t(\partial_\rho x) + \partial_\rho y \partial_t(\partial_\rho y)}{\sqrt{(\partial_\rho x)^2 + (\partial_\rho y)^2}} \\ &= \frac{\partial_\rho \boldsymbol{X}}{|\partial_\rho \boldsymbol{X}|} \cdot \frac{\partial_\rho(\partial_t \boldsymbol{X})}{|\partial_\rho \boldsymbol{X}|} |\partial_\rho \boldsymbol{X}| \\ &= \partial_s \boldsymbol{X} \cdot \partial_s(\partial_t \boldsymbol{X}) |\partial_\rho \boldsymbol{X}|, \end{aligned} \tag{3.12}$$

thus

$$\begin{aligned} \frac{\mathrm{d}}{\mathrm{d}t} \int_{\Gamma(t)} f\,\mathrm{d}s &= \frac{\mathrm{d}}{\mathrm{d}t} \int_0^1 f |\partial_\rho \boldsymbol{X}|\,\mathrm{d}\rho \\ &= \int_0^1 \partial_t f\,|\partial_\rho \boldsymbol{X}| + f\partial_t |\partial_\rho \boldsymbol{X}|\,\mathrm{d}\rho \end{aligned}$$

$$= \int_0^1 \partial_t f\,|\partial_\rho \boldsymbol{X}| + f\,\partial_s(\partial_t \boldsymbol{X})\cdot\partial_s \boldsymbol{X}\,|\partial_\rho \boldsymbol{X}|\,\mathrm{d}\rho \tag{3.13}$$

$$= \int_{\Gamma(t)} \partial_t f + f\,\partial_s(\partial_t \boldsymbol{X})\cdot\partial_s \boldsymbol{X}\,\mathrm{d}s. \quad \square$$

Now the proof of Proposition 3.1 is ready to be presented:

Proof. Denote the region enclosed by $\Gamma(t)$ as $\Omega(t)$. For the area conservation, by the Reynolds' transport theorem [41] and taking $\varphi \equiv 1$ in (3.7a),

$$\begin{aligned}\frac{\mathrm{d}}{\mathrm{d}t}A_c(t) &= \frac{\mathrm{d}}{\mathrm{d}t}\int_{\Omega(t)} 1\,\mathrm{d}x\mathrm{d}y = \int_{\Gamma(t)} \boldsymbol{n}\cdot\partial_t \boldsymbol{X}\,\mathrm{d}s \\ &= \left(\boldsymbol{n}\cdot\partial_t \boldsymbol{X}, 1\right)_{\Gamma(t)} = -\left(\partial_s \mu, \partial_s 1\right)_{\Gamma(t)} = 0.\end{aligned} \tag{3.14}$$

For the energy dissipation part, by Lemma 3.1, we have

$$\begin{aligned}\frac{\mathrm{d}}{\mathrm{d}t}W_c(t) &= \int_{\Gamma(t)} \partial_t \hat{\gamma}(\theta) + \hat{\gamma}(\theta)\partial_s(\partial_t \boldsymbol{X})\cdot\partial_s \boldsymbol{X}\,\mathrm{d}s \\ &= \int_{\Gamma(t)} \hat{\gamma}'(\theta)\partial_t\theta + \hat{\gamma}(\theta)\partial_s(\partial_t \boldsymbol{X})\cdot\partial_s \boldsymbol{X}\,\mathrm{d}s.\end{aligned} \tag{3.15}$$

On the other hand, by using (3.12), we can simplify $\partial_s(\partial_t \boldsymbol{X})$ as

$$\begin{aligned}\partial_s(\partial_t \boldsymbol{X}) &= \frac{1}{|\partial_\rho \boldsymbol{X}|}\partial_\rho(\partial_t \boldsymbol{X}) \\ &= \frac{1}{|\partial_\rho \boldsymbol{X}|}\partial_t\left(|\partial_\rho \boldsymbol{X}|(\cos\theta, \sin\theta)^T\right) \\ &= \frac{1}{|\partial_\rho \boldsymbol{X}|}\left(\partial_s \boldsymbol{X}\cdot\partial_s(\partial_t \boldsymbol{X})|\partial_\rho \boldsymbol{X}|(\cos\theta, \sin\theta)^T + |\partial_\rho \boldsymbol{X}|(-\sin\theta, \cos\theta)^T\partial_t\theta\right)\end{aligned} \tag{3.16}$$

This, together with the fact $\partial_s \boldsymbol{X}^\perp = (\sin\theta, -\cos\theta)^T$, yields that

$$\partial_t\theta = -\partial_s(\partial_t \boldsymbol{X})\cdot\partial_s \boldsymbol{X}^\perp. \tag{3.17}$$

Therefore,

$$\frac{\mathrm{d}}{\mathrm{d}t}W_c(t) = \int_{\Gamma(t)} \left[\hat{\gamma}(\theta)\partial_s \boldsymbol{X} - \hat{\gamma}'(\theta)\partial_s \boldsymbol{X}^\perp\right]\cdot\partial_s(\partial_t \boldsymbol{X})\,\mathrm{d}s. \tag{3.18}$$

Since $\boldsymbol{n}^T\partial_s \boldsymbol{X} \equiv 0$, then

$$\begin{aligned}\hat{\gamma}(\theta)\partial_s \boldsymbol{X} - \hat{\gamma}'(\theta)\partial_s \boldsymbol{X}^\perp &= \hat{\gamma}(\theta)\partial_s \boldsymbol{X} - \hat{\gamma}'(\theta)\partial_s \boldsymbol{X}^\perp + k(\theta)\boldsymbol{n}\boldsymbol{n}^T\partial_s \boldsymbol{X} \\ &= \hat{\boldsymbol{G}}_k(\theta)\partial_s \boldsymbol{X}\end{aligned} \tag{3.19}$$

which leads to

$$\frac{\mathrm{d}}{\mathrm{d}t}W_c(t) = \int_{\Gamma(t)} \hat{\boldsymbol{G}}_k(\theta)\partial_s \boldsymbol{X}\cdot\partial_s(\partial_t \boldsymbol{X})\,\mathrm{d}s. \tag{3.20}$$

Therefore, by taking $\varphi = \mu$ and $\boldsymbol{\omega} = \partial_t \boldsymbol{X}$ in (3.7a) and (3.7b), respectively, we have

$$\begin{aligned}\frac{\mathrm{d}}{\mathrm{d}t}W_c(t) &= \left(\hat{\boldsymbol{G}}_k(\theta)\partial_s \boldsymbol{X}, \partial_s(\partial_t \boldsymbol{X})\right)_{\Gamma(t)} \\ &= \left(\mu\boldsymbol{n}, \partial_t \boldsymbol{X}\right)_{\Gamma(t)} = -\left(\partial_s \mu, \partial_s \mu\right)_{\Gamma(t)} \le 0. \quad \square\end{aligned} \tag{3.21}$$

3.2. A semi-discretization in space

To obtain the spatial discretization, let $N > 2$ be a positive integer and $h = 1/N$ be the mesh size, grid points $\rho_j = jh$, sub-intervals $I_j = [\rho_{j-1}, \rho_j]$ for $j = 1, 2, \cdots, N$ and the uniform partition $\mathbb{I} = [0,1] = \cup_{j=1}^{N} I_j$. The closed curve $\Gamma(t) = \boldsymbol{X}(\cdot, t)$ is approximated by the polygonal curve $\Gamma^h(t) = \boldsymbol{X}^h(\cdot,t) = \left(x^h(\cdot,t), y^h(\cdot,t)\right)^T$ satisfying $\boldsymbol{X}^h(\rho_j, 0) = \boldsymbol{X}(\rho_j, 0)$.

The polygon $\Gamma^h(t)$ is composed of ordered line segments $\{\boldsymbol{h}_j(t)\}_{j=1}^N$, i.e.

$$\Gamma^h(t) = \bigcup_{j=1}^{N} \boldsymbol{h}_j(t) \qquad \text{with} \quad \boldsymbol{h}_j(t) = (h_{j,x}, h_{j,y})^T := \boldsymbol{X}^h(\rho_j, t) - \boldsymbol{X}^h(\rho_{j-1}, t). \tag{3.22}$$

And we always assume that $h_{\min}(t) = \min\limits_{1\le j\le N} |\boldsymbol{h}_j(t)| > 0$ for all $t > 0$.

By using $\boldsymbol{h}_j$, the discrete geometric quantities such as the unit tangential vector $\boldsymbol{\tau}^h$, the outward unit normal vector $\boldsymbol{n}^h$ and the inclination angle θ^h can be computed on each segment as:

$$\boldsymbol{\tau}^h|_{I_j} = \frac{\boldsymbol{h}_j}{|\boldsymbol{h}_j|} := \boldsymbol{\tau}_j^h, \qquad \boldsymbol{n}^h|_{I_i} = -(\boldsymbol{\tau}_j^h)^{\perp} = -\frac{(\boldsymbol{h}_j)^{\perp}}{|\boldsymbol{h}_j|} := \boldsymbol{n}_j^h; \tag{3.23}$$

and

$$\theta^h|_{I_j} := \theta_j^h, \qquad \text{satisfying} \quad \cos\theta_j^h = \frac{h_{j,x}}{|\boldsymbol{h}_j|}, \quad \sin\theta_j^h = \frac{h_{j,y}}{|\boldsymbol{h}_j|}. \tag{3.24}$$

We introduce the finite element subspaces

$$\mathbb{K}^h := \left\{ u^h \in C(\mathbb{I}) \mid u^h|_{I_j} \in \mathcal{P}^1(I_j),\ \forall j = 1, 2, \cdots, N \right\} \subseteq H^1(\mathbb{I}), \tag{3.25a}$$

$$\mathbb{K}_p^h := \{u^h \in \mathbb{K}^h \mid u^h(0) = u^h(1)\}, \qquad \mathbb{X}_p^h := [H_p^1(\mathbb{I})]^2, \tag{3.25b}$$

where $\mathcal{P}^1(I_j)$ is the set of polynomials defined on I_j of degree ≤ 1. For $u, v \in \mathbb{K}^h$, the mass-lumped inner product $\left(\cdot,\cdot\right)_{\Gamma^h(t)}^h$ with respect to $\Gamma^h(t)$ is defined as

$$\left(u, v\right)_{\Gamma^h(t)}^h := \frac{1}{2}\sum_{j=1}^{N} |\boldsymbol{h}_j(t)| \left((u\cdot v)(\rho_{j-1}^+) + (u\cdot v)(\rho_j^-) \right), \tag{3.26}$$

where $u(\rho_j^{\pm}) = \lim\limits_{\rho\to\rho_j^{\pm}} u(\rho)$. And the discretized differential operator ∂_s for $f \in \mathbb{K}^h$ is defined as

$$\partial_s f|_{I_j} := \frac{f(\rho_j) - f(\rho_{j-1})}{|\boldsymbol{h}_j|}. \tag{3.27}$$

The above definitions also hold true for vector-valued functions.

We now propose the spatial semi-discretization for (3.7) as follows: Let $\Gamma_0^h := \boldsymbol{X}^h(\cdot,0) \in \mathbb{X}_p^h, \mu(\cdot) \in \mathbb{K}_p^h$ be the approximations of $\Gamma_0 := \boldsymbol{X}_0(\cdot), \mu_0(\cdot)$, respectively, for $t > 0$, find the solution $\left(\boldsymbol{X}^h(\cdot,t), \mu^h(\cdot)\right) \in \mathbb{X}_p^h \times \mathbb{K}_p^h$ such that

$$\left(\boldsymbol{n}^h \cdot \partial_t \boldsymbol{X}^h, \varphi^h\right)_{\Gamma^h(t)}^h + \left(\partial_s \mu^h, \partial_s \varphi^h\right)_{\Gamma^h(t)}^h = 0, \qquad \forall \varphi^h \in \mathbb{K}_p^h, \tag{3.28a}$$

$$\left(\mu^h \boldsymbol{n}^h, \boldsymbol{\omega}^h\right)_{\Gamma^h(t)}^h - \left(\hat{\boldsymbol{G}}_k(\theta^h)\partial_s \boldsymbol{X}^h, \partial_s \boldsymbol{\omega}^h\right)_{\Gamma^h(t)}^h = 0, \qquad \forall \boldsymbol{\omega}^h \in \mathbb{X}_p^h, \tag{3.28b}$$

where

$$\hat{\boldsymbol{G}}_k(\theta^h) = \begin{pmatrix} \hat{\gamma}(\theta^h) & -\hat{\gamma}'(\theta^h) \\ \hat{\gamma}'(\theta^h) & \hat{\gamma}(\theta^h) \end{pmatrix} + k(\theta^h) \begin{pmatrix} \sin^2\theta^h & -\cos\theta^h \sin\theta^h \\ -\cos\theta^h \sin\theta^h & \cos^2\theta^h \end{pmatrix}. \tag{3.29}$$

Denote the enclosed area and the free energy of the polygonal curve $\Gamma^h(t)$ as $A_c^h(t)$ and $W_c^h(t)$, respectively, which are given by

$$A_c^h(t) = \frac{1}{2}\sum_{j=1}^{N} (x_j^h(t) - x_{j-1}^h(t))(y_j^h(t) + y_{j-1}^h(t)), \tag{3.30a}$$

$$W_c^h(t) = \sum_{j=1}^{N} |\boldsymbol{h}_j(t)| \hat{\gamma}(\theta_j^h), \tag{3.30b}$$

where $x_j^h(t) := x^h(\rho_j, t), y_j^h(t) := y^h(\rho_j, t),\ \forall 0 \le j \le N$.

Following similar steps in Proposition 3.1, it can be proved that the two geometric properties for the semi-discretization (3.28) still preserve:

Proposition 3.2 *(Area conservation and energy dissipation). Suppose $\Gamma^h(t)$ is given by the solution $(\boldsymbol{X}^h(\cdot,t),\mu^h(\cdot,t))$ of (3.28), then we have*

$$A_c^h(t)\equiv A_c^h(0),\quad W_c^h(t)\le W_c^h(t_1)\le W_c^h(0),\quad \forall t\ge t_1\ge 0. \tag{3.31}$$

3.3. A structure-preserving SPFEM discretization

Let τ be the uniform time step. Denoting the approximation of $\Gamma(t)=\boldsymbol{X}(\cdot,t)$ at $t_m=m\tau, m=0,1,\cdots$, as $\Gamma^m=\boldsymbol{X}^m(\cdot)=\cup_{j=1}^N \boldsymbol{h}_j^m$ where $\boldsymbol{h}_j^m:=\boldsymbol{X}^m(\rho_j)-\boldsymbol{X}^m(\rho_{j-1})$. Then the definitions of the mass lumped inner product $(\cdot,\cdot)^h_{\Gamma^m}$, the unit tangential vector $\boldsymbol{\tau}^m$, the unit outward normal vector $\boldsymbol{n}^m$, and the inclination angle θ^m with respect to Γ^m can be given in a similar approach.

Following the ideas in [3,5,11,34] to design an SP-PFEM for surface diffusion, we utilize the explicit-implicit Euler method in time. The derived fully-implicit structure-preserving discretization of SPFEM for the anisotropic surface diffusion (2.1) is expressed as follows:

Suppose the initial approximation $\Gamma^0(\cdot)\in\mathbb{X}^h$ is given by $\boldsymbol{X}^0(\rho_j)=\boldsymbol{X}_0(\rho_j),\forall 0\le j\le N$. For any $m=0,1,2,\ldots$, find the solution $(\boldsymbol{X}^{m+1}(\cdot)=(x^{m+1}(\cdot),y^{m+1}(\cdot))^T,\mu^{m+1}(\cdot))\in\mathbb{X}_p^h\times\mathbb{K}_p^h$ such that

$$\left(\boldsymbol{n}^{m+\frac12}\cdot\frac{\boldsymbol{X}^{m+1}-\boldsymbol{X}^m}{\tau},\varphi^h\right)^h_{\Gamma^m}+\left(\partial_s\mu^{m+1},\partial_s\varphi^h\right)^h_{\Gamma^m}=0,\qquad \forall\varphi^h\in\mathbb{K}_p^h, \tag{3.32a}$$

$$\left(\mu^{m+1}\boldsymbol{n}^{m+\frac12},\boldsymbol{\omega}^h\right)^h_{\Gamma^m}-\left(\hat{\boldsymbol{G}}_k(\theta^m)\partial_s\boldsymbol{X}^{m+1},\partial_s\boldsymbol{\omega}^h\right)^h_{\Gamma^m}=0,\qquad \forall\boldsymbol{\omega}^h\in\mathbb{X}_p^h, \tag{3.32b}$$

where

$$\hat{\boldsymbol{G}}_k(\theta^m)=\begin{pmatrix}\hat\gamma(\theta^m) & -\hat\gamma'(\theta^m)\\ \hat\gamma'(\theta^m) & \hat\gamma(\theta^m)\end{pmatrix}+k(\theta^m)\begin{pmatrix}\sin^2\theta^m & -\cos\theta^m\sin\theta^m\\ -\cos\theta^m\sin\theta^m & \cos^2\theta^m\end{pmatrix}, \tag{3.33}$$

and

$$\boldsymbol{n}^{m+\frac12}:=-\frac12\frac{1}{|\partial_\rho\boldsymbol{X}^m|}(\partial_\rho\boldsymbol{X}^m+\partial_\rho\boldsymbol{X}^{m+1})^\perp. \tag{3.34}$$

Remark 3.1. The above scheme is weakly implicit, as the integral domain is explicitly chosen and each equation contains only one non-linear term. The nonlinear term is a polynomial function of degree ≤ 2 with respect to the components of $\boldsymbol{X}^{m+1}$ and μ^{m+1}, thus it can be efficiently and accurately solved by the Newton's iterative method similar to [11].

Remark 3.2. The choice of $\boldsymbol{n}^{m+\frac12}$ is crucial for maintaining the area conservation. The scheme becomes semi-implicit if $\boldsymbol{n}^{m+\frac12}$ is replaced by $\boldsymbol{n}^m$, and only the energy dissipation property is preserved.

3.4. Main results

Denote the enclosed area and the free energy of the polygon Γ^m as A_c^m and W_c^m, respectively, which are given by

$$A_c^m=\frac12\sum_{j=1}^N\left(x^m(\rho_j)-x^m(\rho_{j-1})\right)\left(y^m(\rho_j)+y^m(\rho_{j-1})\right), \tag{3.35a}$$

$$W_c^m=\sum_{j=1}^N|\boldsymbol{h}_j^m|\hat\gamma(\theta_j^m). \tag{3.35b}$$

In practical applications, it's common to encounter situations where $\hat\gamma(\theta)$ lacks high regularity. In the following sections, we always assume that $\hat\gamma(\theta)$ is globally C^1 and piecewise C^2 on $2\pi\mathbb{T}$.

We thus introduce the following energy stable conditions on $\hat\gamma(\theta)$:

Definition 3.1 *(Energy stable condition).* Suppose $\hat\gamma(\theta)$ is globally C^1 and piecewise C^2, the energy stable conditions on $\hat\gamma(\theta)$ are given as follows:

$$3\hat\gamma(\theta)\ge\hat\gamma(\theta-\pi),\qquad\forall\theta\in2\pi\mathbb{T}, \tag{3.36a}$$

$$\hat\gamma'(\theta^*)=0,\ \text{when } 3\hat\gamma(\theta^*)=\hat\gamma(\theta^*-\pi),\qquad\theta^*\in2\pi\mathbb{T}. \tag{3.36b}$$

The main result of this work is the following structure-preserving property of the SPFEM (3.32):

Theorem 3.1 *(Structure-preserving). For any $\hat{\gamma}(\theta)$ satisfying (3.36), the SPFEM (3.32) is area conservative and unconditional energy dissipative with sufficiently large $k(\theta)$, i.e.*

$$A_c^{m+1} = A_c^m = \cdots = A_c^0, \qquad W_c^{m+1} \le W_c^m \le \cdots \le W_c^0, \qquad \forall m \ge 0. \tag{3.37}$$

The proof of area conservation part is analogous to [11, Theorem 2.1], we omit here for brevity. And the energy dissipation will be established in the next section.

Remark 3.3. The SPFEM (3.32) is a numerical algorithm designed for the sharp interface model, stabilization techniques for the phase-field model, such as convex splitting scheme [27,45], stabilized semi-implicit scheme [19,22], etc, do not apply here. Different from these classical stabilization schemes in phase-field methods, the SPFEM (3.32) can maintain the original energy stability, without requiring additional correction terms.

Remark 3.4. For the m-fold anisotropy (1.6): the energy stable condition (3.36) holds when $|\beta| < 1$ and $|\beta| \le \frac{1}{2}$ for m being even and odd, respectively. It is a significant improvement compared to the energy stable condition $|\beta| \le \frac{1}{m^2+1}$ in [36].

Remark 3.5. For the ellipsoidal anisotropy (1.7): the energy stable condition in [36] requires $-\frac{a}{2} \le b \le a$; while condition (3.36) is satisfied for any $a > 0, a + b > 0$.

Remark 3.6. It is noteworthy that for any symmetric anisotropy $\hat{\gamma}(\theta)$ satisfying $\hat{\gamma}(\theta) = \hat{\gamma}(\theta - \pi)$, $\forall \theta \in 2\pi\mathbb{T}$, such as the Riemannian-like metric anisotropy (1.8), condition (3.36) naturally holds. Thereby it ensures the unconditional energy stability of the SPFEM (3.32).

4. Unconditionally energy stability of the SPFEM

The key point in proving energy dissipation of (3.32) is to establish an energy estimate akin to

$$\left(\hat{\boldsymbol{G}}_k(\theta^m)\partial_s \boldsymbol{X}^{m+1}, \partial_s(\boldsymbol{X}^{m+1} - \boldsymbol{X}^m)\right)_{\Gamma^m}^h \ge W_c^{m+1} - W_c^m, \tag{4.1}$$

for controlling the energy difference between two subsequent time steps with the surface energy matrix $\boldsymbol{G}_k$. To achieve desired inequality, we need a local version of the estimate, which is formulated by the following lemma:

Lemma 4.1 *(Local energy estimate). Suppose $\boldsymbol{h}, \hat{\boldsymbol{h}}$ are two non-zero vectors in $\mathbb{R}^2$. Let $\boldsymbol{n} = -\frac{\boldsymbol{h}^\perp}{|\boldsymbol{h}|} = (-\sin\theta, \cos\theta)^T$ and $\hat{\boldsymbol{n}} = -\frac{\hat{\boldsymbol{h}}^\perp}{|\hat{\boldsymbol{h}}|} = (-\sin\hat{\theta}, \cos\hat{\theta})^T$ be the corresponding unit normal vectors. Then for sufficiently large $k(\theta)$, the following inequality holds*

$$\frac{1}{|\boldsymbol{h}|}\left(\hat{\boldsymbol{G}}_k(\theta)\hat{\boldsymbol{h}}\right) \cdot (\hat{\boldsymbol{h}} - \boldsymbol{h}) \ge |\hat{\boldsymbol{h}}|\hat{\gamma}(\hat{\theta}) - |\boldsymbol{h}|\hat{\gamma}(\theta). \tag{4.2}$$

Remark 4.1. It is noteworthy to mention that the condition (3.36) is almost sufficient to the local energy estimate. Let $\hat{\boldsymbol{h}} = -\boldsymbol{h}$ and $\hat{\theta} = \theta - \pi$. Consequently, the inequality (4.2) becomes $2|\boldsymbol{h}|\hat{\gamma}(\theta) \ge |\boldsymbol{h}|\hat{\gamma}(\theta - \pi) - |\boldsymbol{h}|\hat{\gamma}(\theta)$. Therefore, our energy stability condition (3.36) proves to be almost essential for the local energy estimate.

4.1. The minimal stabilizing function and its properties

To prove the local energy estimate (4.2), the following two auxiliary functions are introduced as:

$$P_\alpha(\phi, \theta) := 2\sqrt{\hat{\gamma}^2(\theta) + \alpha\hat{\gamma}(\theta)\sin^2\phi}, \qquad \forall \phi \in 2\pi\mathbb{T}, \tag{4.3a}$$

$$Q(\phi, \theta) := \hat{\gamma}(\theta - \phi) + \hat{\gamma}(\theta)\cos\phi + \hat{\gamma}'(\theta)\sin\phi, \qquad \forall \phi \in 2\pi\mathbb{T}. \tag{4.3b}$$

With the help of P_α, Q, we present the definition of minimal stabilizing function as follows:

$$k_0(\theta) := \inf\left\{\alpha \ge 0 \mid P_\alpha(\phi, \theta) - Q(\phi, \theta) \ge 0,\ \forall \phi \in 2\pi\mathbb{T}\right\}. \tag{4.4}$$

We note that the function $k_0(\theta)$ is determined by $\hat{\gamma}(\theta)$, making it time-independent. In numerical experiments, this allows $k_0(\theta)$ to be pre-allocated for efficiency.

The following theorem guarantees the existence of $k_0(\theta)$:

Theorem 4.1. *For $\hat{\gamma}(\theta)$ satisfying (3.36), the minimal stabilizing function $k_0(\theta)$, as given in (4.4), is well-defined.*

The proof of Theorem 4.1 will be presented in Section 5.

Once the $\hat{\gamma}(\theta)$ is given, the minimal stabilizing function $k_0(\theta)$ is determined, inducing a mapping from $\hat{\gamma}(\theta)$ to $k_0(\theta)$. Moreover, this mapping is sublinear, i.e., it is positive homogeneity and subadditivity.

4.2. Proof of the local energy estimate

Proof. Applying the definitions of $\hat{\boldsymbol{G}}_k(\theta)$ in (2.4), noting that

$$\begin{pmatrix} \sin^2\theta & -\cos\theta\sin\theta \\ -\cos\theta\sin\theta & \cos^2\theta \end{pmatrix} = \begin{pmatrix} -\sin\theta \\ \cos\theta \end{pmatrix} (-\sin\theta, \cos\theta) = \boldsymbol{n}\boldsymbol{n}^T, \tag{4.5}$$

then we have

$$\begin{aligned} \frac{1}{|\boldsymbol{h}|}\left(\hat{\boldsymbol{G}}_k(\theta)\hat{\boldsymbol{h}}\right)\cdot\hat{\boldsymbol{h}} &= \frac{1}{|\boldsymbol{h}|}\left[\hat{\gamma}(\theta)I_2 + \hat{\gamma}'(\theta)J + k(\theta)\boldsymbol{n}\boldsymbol{n}^T\right]\hat{\boldsymbol{h}}\cdot\hat{\boldsymbol{h}} \\ &= \frac{1}{|\boldsymbol{h}|}\hat{\gamma}(\theta)|\hat{\boldsymbol{h}}|^2 + \frac{1}{|\boldsymbol{h}|}\hat{\gamma}'(\theta)J\hat{\boldsymbol{h}}\cdot\hat{\boldsymbol{h}} + \frac{1}{|\boldsymbol{h}|}k(\theta)(\boldsymbol{n}\cdot\hat{\boldsymbol{h}})^2 \\ &= \frac{1}{|\boldsymbol{h}|}\hat{\gamma}(\theta)|\hat{\boldsymbol{h}}|^2 + \frac{1}{|\boldsymbol{h}|}k(\theta)(\boldsymbol{n}\cdot\hat{\boldsymbol{h}})^2 \\ &= \frac{1}{|\boldsymbol{h}|}\left[\hat{\gamma}(\theta) + k(\theta)\sin^2(\theta-\hat{\theta})\right]|\hat{\boldsymbol{h}}|^2, \end{aligned} \tag{4.6}$$

and

$$\begin{aligned} \frac{1}{|\boldsymbol{h}|}\left(\hat{\boldsymbol{G}}_k(\theta)\hat{\boldsymbol{h}}\right)\cdot\boldsymbol{h} &= \frac{1}{|\boldsymbol{h}|}\left[\hat{\gamma}(\theta)I_2 + \hat{\gamma}'(\theta)J + k(\theta)\boldsymbol{n}\boldsymbol{n}^T\right]\hat{\boldsymbol{h}}\cdot\boldsymbol{h} \\ &= \frac{1}{|\boldsymbol{h}|}\hat{\gamma}(\theta)(\boldsymbol{h}\cdot\hat{\boldsymbol{h}}) + \frac{1}{|\boldsymbol{h}|}\hat{\gamma}'(\theta)J\hat{\boldsymbol{h}}\cdot\boldsymbol{h} + \frac{1}{|\boldsymbol{h}|}k(\theta)\boldsymbol{n}\boldsymbol{n}^T\hat{\boldsymbol{h}}\cdot\boldsymbol{h} \\ &= |\hat{\boldsymbol{h}}|\hat{\gamma}(\theta)\begin{pmatrix}\cos\theta\\ \sin\theta\end{pmatrix}\cdot\begin{pmatrix}\cos\hat{\theta}\\ \sin\hat{\theta}\end{pmatrix} + |\hat{\boldsymbol{h}}|\hat{\gamma}'(\theta)\begin{pmatrix}0 & -1\\ 1 & 0\end{pmatrix}\begin{pmatrix}\cos\hat{\theta}\\ \sin\hat{\theta}\end{pmatrix}\cdot\begin{pmatrix}\cos\theta\\ \sin\theta\end{pmatrix} \\ &\quad + |\hat{\boldsymbol{h}}|k(\theta)\begin{pmatrix}\sin^2\theta & -\cos\theta\sin\theta\\ -\cos\theta\sin\theta & \cos^2\theta\end{pmatrix}\begin{pmatrix}\cos\hat{\theta}\\ \sin\hat{\theta}\end{pmatrix}\cdot\begin{pmatrix}\cos\theta\\ \sin\theta\end{pmatrix} \\ &= |\hat{\boldsymbol{h}}|\hat{\gamma}(\theta)\cos(\theta-\hat{\theta}) + |\hat{\boldsymbol{h}}|\hat{\gamma}'(\theta)(-\sin\hat{\theta},\cos\hat{\theta})\cdot(\cos\theta,\sin\theta) \\ &= |\hat{\boldsymbol{h}}|\left[\hat{\gamma}(\theta)\cos(\theta-\hat{\theta}) + \hat{\gamma}'(\theta)\sin(\theta-\hat{\theta})\right]. \end{aligned} \tag{4.7}$$

Recall the definitions of $P_\alpha(\phi,\theta), Q(\phi,\theta)$ in (4.3), we have

$$\frac{1}{|\boldsymbol{h}|}\left(\hat{\boldsymbol{G}}_k(\theta)\hat{\boldsymbol{h}}\right)\cdot\hat{\boldsymbol{h}} = \frac{|\hat{\boldsymbol{h}}|^2}{4|\boldsymbol{h}|\hat{\gamma}(\theta)}P^2_{k(\theta)}(\phi,\theta), \tag{4.8a}$$

$$\frac{1}{|\boldsymbol{h}|}\left(\hat{\boldsymbol{G}}_k(\theta)\hat{\boldsymbol{h}}\right)\cdot\boldsymbol{h} = |\hat{\boldsymbol{h}}|(Q(\phi,\theta) - \hat{\gamma}(\theta-\phi)), \tag{4.8b}$$

with $\phi = \theta - \hat{\theta}$.

Substituting (4.8a), (4.8b) into the local energy estimate (4.2), we have

$$\begin{aligned} &\frac{1}{|\boldsymbol{h}|}\left(\hat{\boldsymbol{G}}_k(\theta)\hat{\boldsymbol{h}}\right)\cdot(\hat{\boldsymbol{h}}-\boldsymbol{h}) - \left(|\hat{\boldsymbol{h}}|\hat{\gamma}(\hat{\theta}) - |\boldsymbol{h}|\hat{\gamma}(\theta)\right) \\ &\quad= \frac{|\hat{\boldsymbol{h}}|^2}{4|\boldsymbol{h}|\hat{\gamma}(\theta)}P^2_{k(\theta)}(\phi,\theta) - |\hat{\boldsymbol{h}}|(Q(\phi,\theta) - \hat{\gamma}(\theta-\phi)) \\ &\qquad - |\hat{\boldsymbol{h}}|\hat{\gamma}(\theta-\phi) + |\boldsymbol{h}|\hat{\gamma}(\theta) \\ &\quad= \frac{1}{4|\boldsymbol{h}|\hat{\gamma}(\theta)}\left[|\hat{\boldsymbol{h}}|^2P^2_{k(\theta)}(\phi,\theta) - 4|\hat{\boldsymbol{h}}||\boldsymbol{h}|\hat{\gamma}(\theta)Q(\phi,\theta) + 4|\boldsymbol{h}|^2\hat{\gamma}^2(\theta)\right], \end{aligned} \tag{4.9}$$

thus the local energy estimate (4.2) is equivalent to

$$|\hat{\boldsymbol{h}}|^2P^2_{k(\theta)}(\phi,\theta) - 4|\hat{\boldsymbol{h}}||\boldsymbol{h}|\hat{\gamma}(\theta)Q(\phi,\theta) + 4|\boldsymbol{h}|^2\hat{\gamma}^2(\theta) \geq 0. \tag{4.10}$$

i.e.

$$\left(|\hat{\boldsymbol{h}}|P_{k(\theta)} - 2|\boldsymbol{h}|\hat{\gamma}(\theta)\right)^2 + 4|\hat{\boldsymbol{h}}||\boldsymbol{h}|\hat{\gamma}(\theta)\left(P_{k(\theta)}(\phi,\theta) - Q(\phi,\theta)\right) \geq 0 \tag{4.11}$$

By the definition (4.4) of $k_0(\theta)$, we have $P_{k(\theta)}(\phi,\theta) - Q(\phi,\theta) \geq 0$, $\forall\phi \in 2\pi\mathbb{T}$ for any $k(\theta) \geq k_0(\theta)$, thus (4.11) holds true. By Theorem 4.1, the minimal stabilizing function $k_0(\theta) < +\infty$ is well-defined, therefore we can choose sufficiently large $k(\theta) \geq k_0(\theta)$ such that the intended local energy estimate (4.2) is validated. □

4.3. Proof of the main result

Leveraging the local energy estimate (4.2) as outlined in Lemma 4.1, we can now prove the unconditional energy stability aspect of the main result, as stated in Theorem 3.1.

Proof. Suppose $k(\theta)$ is sufficiently large such that $k(\theta) \geq k_0(\theta)$. We take $\boldsymbol{h} = \boldsymbol{h}_j^m, \hat{\boldsymbol{h}} = \boldsymbol{h}_j^{m+1}$ in the local energy estimate (4.2):

$$\frac{1}{|\boldsymbol{h}_j^m|}\left(\hat{\boldsymbol{G}}_k(\theta_j^m)\boldsymbol{h}_j^{m+1}\right)\cdot(\boldsymbol{h}_j^{m+1}-\boldsymbol{h}_j^m) \geq |\boldsymbol{h}_j^{m+1}|\hat{\gamma}(\theta_j^{m+1}) - |\boldsymbol{h}_j^m|\hat{\gamma}(\theta_j^m). \tag{4.12}$$

Therefore, for any $m \geq 0$,

$$\begin{aligned}
\left(\hat{\boldsymbol{G}}_k(\theta^m)\partial_s\boldsymbol{X}^{m+1}, \partial_s(\boldsymbol{X}^{m+1}-\boldsymbol{X}^m)\right)_{\Gamma^m}^h &= \sum_{j=1}^N\left[|\boldsymbol{h}_j^m|\left(\hat{\boldsymbol{G}}_k(\theta_j^m)\frac{\boldsymbol{h}_j^{m+1}}{|\boldsymbol{h}_j^m|}\right)\cdot\frac{\boldsymbol{h}_j^{m+1}-\boldsymbol{h}_j^m}{|\boldsymbol{h}_j^m|}\right]\\
&= \sum_{j=1}^N\left[\frac{1}{|\boldsymbol{h}_j^m|}\left(\hat{\boldsymbol{G}}_k(\theta_j^m)\boldsymbol{h}_j^{m+1}\right)\cdot(\boldsymbol{h}_j^{m+1}-\boldsymbol{h}_j^m)\right]\\
&\geq \sum_{j=1}^N\left[|\boldsymbol{h}_j^{m+1}|\hat{\gamma}(\theta_j^{m+1}) - |\boldsymbol{h}_j^m|\hat{\gamma}(\theta_j^m)\right]\\
&= \sum_{j=1}^N|\boldsymbol{h}_j^{m+1}|\hat{\gamma}(\theta_j^{m+1}) - \sum_{j=1}^N|\boldsymbol{h}_j^m|\hat{\gamma}(\theta_j^m)\\
&= W_c^{m+1} - W_c^m.
\end{aligned} \tag{4.13}$$

Taking $\varphi^h = \mu^{m+1}, \boldsymbol{\omega}^h = \boldsymbol{X}^{m+1}-\boldsymbol{X}^m$ in (3.32), we have

$$\begin{aligned}
\left(\hat{\boldsymbol{G}}_k(\theta^m)\partial_s\boldsymbol{X}^{m+1}, \partial_s(\boldsymbol{X}^{m+1}-\boldsymbol{X}^m)\right)_{\Gamma^m}^h &= \left(\mu^{m+1}\boldsymbol{n}^{m+\frac{1}{2}}, \boldsymbol{X}^{m+1}-\boldsymbol{X}^m\right)_{\Gamma^m}^h\\
&= -\tau\left(\partial_s\mu^{m+1}, \partial_s\mu^{m+1}\right)_{\Gamma^m}^h.
\end{aligned} \tag{4.14}$$

Combining this with (4.13) yields that

$$\begin{aligned}
W_c^{m+1} - W_c^m &\leq \left(\hat{\boldsymbol{G}}_k(\theta^m)\partial_s\boldsymbol{X}^{m+1}, \partial_s(\boldsymbol{X}^{m+1}-\boldsymbol{X}^m)\right)_{\Gamma^m}^h\\
&\leq -\tau\left(\partial_s\mu^{m+1}, \partial_s\mu^{m+1}\right)_{\Gamma^m}^h\\
&\leq 0, \qquad \forall m \geq 0,
\end{aligned} \tag{4.15}$$

which immediately implies the unconditional energy stability in (3.37). □

5. Existence of the minimal stabilizing function

In this section, we present a proof of the existence of the minimal stabilizing function corresponding to $\hat{\gamma}(\theta)$ that satisfies the energy stable condition in (3.36).

Recall the definition (4.3) of P_α, Q, denote

$$\begin{aligned}
F_\alpha(\phi,\theta) &:= P_\alpha^2(\phi,\theta) - Q^2(\phi,\theta)\\
&= 4\hat{\gamma}(\theta)\left(\hat{\gamma}(\theta)+\alpha\sin^2\phi\right) - \left(\hat{\gamma}(\theta-\phi)+\hat{\gamma}(\theta)\cos\phi+\hat{\gamma}'(\theta)\sin\phi\right)^2.
\end{aligned} \tag{5.1}$$

Suppose $C > 0$ is a positive number such that $\frac{1}{C} \leq \hat{\gamma}(\theta) \leq C$ and $|\hat{\gamma}'(\theta)|, |\hat{\gamma}''(\theta)| \leq C,\ \forall\theta \in 2\pi\mathbb{T}$.

Before formally commencing our proof, we first need the following two technical lemmas:

Lemma 5.1. *For a globally C^1 and piecewise C^2 anisotropy $\hat{\gamma}(\theta)$, there exists an open neighborhood U_0 of 0 and a positive constant $k_{U_0} < +\infty$ such that for any $\alpha > k_{U_0}$, we have $F_\alpha(\phi,\theta) \geq 0, \forall\phi \in U_0$.*

Proof. Since $\hat{\gamma}(\theta)$ is globally C^1 and piecewise C^2, there exists a $0 < \varepsilon < \frac{\pi}{2}$ such that $\hat{\gamma}(\theta)$ is 2-times continuously differentiable on both $[\theta-\varepsilon, \theta]$ and $[\theta, \theta+\varepsilon]$.

Applying the mean value theorem to $[\theta-\varepsilon, \theta]$ and $[\theta, \theta+\varepsilon]$, we deduce that for $\phi \in U_0 := \{\phi \mid |\phi| < \varepsilon\}$, there exists a ξ between θ and $\theta-\phi$ such that

$$\hat{\gamma}(\theta-\phi) = \hat{\gamma}(\theta) - \hat{\gamma}'(\theta)\phi + \frac{\hat{\gamma}''(\xi)}{2}\phi^2. \tag{5.2}$$

Again, by the mean value theorem, there exist ξ_1, ξ_2 between $0, \phi$ such that

$$\cos\phi = 1 - \frac{1}{2}\phi^2 + \frac{\sin\xi_1}{6}\phi^3 \tag{5.3a}$$

$$\sin\phi = \phi - \frac{\cos\xi_2}{6}\phi^3. \tag{5.3b}$$

Substituting (5.2) and (5.3) into $2\hat{\gamma}(\theta) - Q(\phi,\theta)$, we have

$$\begin{aligned} 2\hat{\gamma}(\theta) - Q(\phi,\theta) &= 2\hat{\gamma}(\theta) - \hat{\gamma}(\theta) + \hat{\gamma}'(\theta)\phi - \frac{1}{2}\hat{\gamma}''(\xi)\phi^2 \\ &\quad - \hat{\gamma}(\theta) + \frac{1}{2}\hat{\gamma}(\theta)\phi^2 - \frac{1}{6}\hat{\gamma}(\theta)\sin\xi_1\phi^3 \\ &\quad - \hat{\gamma}'(\theta)\phi + \frac{1}{6}\hat{\gamma}'(\theta)\cos\xi_2\phi^3 \\ &= \frac{1}{2}\left(\hat{\gamma}(\theta) - \hat{\gamma}''(\xi)\right)\phi^2 - \frac{1}{6}\left(\hat{\gamma}(\theta)\sin\xi_1 - \hat{\gamma}'(\theta)\cos\xi_2\right)\phi^3. \end{aligned} \tag{5.4}$$

Thus,

$$\begin{aligned} |2\hat{\gamma}(\theta) - Q(\phi,\theta)| &\le \frac{1}{2}\left(|\hat{\gamma}(\theta)| + |\hat{\gamma}''(\xi)|\right)|\phi|^2 \\ &\quad + \frac{1}{6}\left(|\hat{\gamma}(\theta)\sin\xi_1| + |\hat{\gamma}'(\theta)\cos\xi_2|\right)|\phi|^3 \\ &\le C|\phi|^2 + \frac{C}{3}|\phi|^3. \end{aligned} \tag{5.5}$$

Since $|2\hat{\gamma}(\theta) + Q(\phi,\theta)| \le 2|\hat{\gamma}(\theta)| + |Q(\phi,\theta)| \le 5C$, then for any $\phi \in U_0$,

$$\begin{aligned} |4\hat{\gamma}^2(\theta) - Q^2(\phi,\theta)| &\le |2\hat{\gamma}(\theta) + Q(\phi,\theta)||2\hat{\gamma}(\theta) - Q(\phi,\theta)| \\ &\le 5C\left(C|\phi|^2 + \frac{C}{3}|\phi|^3\right) \\ &= \frac{5C^2}{3}(3 + |\phi|)|\phi|^2 \\ &\le \frac{5(6+\pi)C^2}{6}|\phi|^2. \end{aligned} \tag{5.6}$$

Noting that for any $\phi \in U_0$, we have $|\sin\phi| > \frac{2}{\pi}|\phi|$, therefore,

$$\begin{aligned} F_\alpha(\phi,\theta) &= 4\hat{\gamma}(\theta)\alpha\sin^2\phi + 4\hat{\gamma}^2(\theta) - Q^2(\phi,\theta) \\ &\ge \frac{16}{C\pi^2}\alpha|\phi|^2 - \frac{5(6+\pi)C^2}{6}|\phi|^2 \\ &\ge \left[\frac{16}{C\pi^2}\alpha - \frac{5(6+\pi)C^2}{6}\right]|\phi|^2,\ \forall\phi \in U_0. \end{aligned} \tag{5.7}$$

Thus there exists a positive constant $k_{U_0} := \frac{5\pi^2(6+\pi)C^3}{96}$, for $\alpha > k_{U_0}$, $F_\alpha(\phi,\theta) \ge 0, \forall\phi \in U_0$. □

Lemma 5.2. *Suppose $\hat{\gamma}(\theta)$ satisfying (3.36). There exists an open neighborhood U_π of π with a positive $k_{U_\pi} < +\infty$ such that for any $\alpha > k_{U_\pi}$, $F_\alpha(\phi,\theta) \ge 0, \forall\phi \in U_\pi$.*

Proof. (i) If $3\hat{\gamma}(\theta) > \hat{\gamma}(\theta - \pi)$ for any $\theta \in 2\pi\mathbb{T}$, then

$$F_\alpha(\pi,\theta) = (3\hat{\gamma}(\theta) - \hat{\gamma}(\theta-\pi))(\hat{\gamma}(\theta) + \hat{\gamma}(\theta-\pi)) > 0. \tag{5.8}$$

Thus, by the continuity of $F_\alpha(\phi,\theta)$, there exists an open neighborhood U_π of π such that $F_\alpha(\pi,\theta) \ge 0, \forall\phi \in U_\pi$.

(ii) If $3\hat{\gamma}(\theta^*) = \hat{\gamma}(\theta^* - \pi)$ and $\hat{\gamma}'(\theta^*) = 0$ at $\theta^* \in 2\pi\mathbb{T}$. Since function $\gamma(\theta-\pi)/\gamma(\theta) \le 3$, it attends its maximum at θ^*, thus

$$\begin{aligned} \left(\frac{\hat{\gamma}(\theta-\pi)}{\hat{\gamma}(\theta)}\right)'\Bigg|_{\theta=\theta^*} &= \frac{\hat{\gamma}'(\theta^*-\pi)\hat{\gamma}(\theta^*) - \hat{\gamma}(\theta^*-\pi)\hat{\gamma}'(\theta^*)}{\hat{\gamma}^2(\theta^*)} \\ &= \frac{\hat{\gamma}'(\theta^*-\pi) - 3\hat{\gamma}'(\theta^*)}{\hat{\gamma}(\theta^*)} \\ &= \frac{\hat{\gamma}'(\theta^*-\pi)}{\hat{\gamma}(\theta^*)} = 0, \end{aligned} \tag{5.9}$$

i.e., $\hat{\gamma}'(\theta^* - \pi) = 0$.

Similar to derivations of (5.2), according to the mean value theorem, we know that there exists positive number $0 < \varepsilon < \frac{\pi}{2}$ and a neighborhood $U_\pi = \{\phi \mid |\phi - \pi| < \varepsilon\}$. Such that for any $\phi \in U_\pi$, there exists a ξ between $\theta^* - \phi$ and $\theta^* - \pi$ satisfying

$$\begin{aligned}\hat{\gamma}(\theta^* - \phi) &= \hat{\gamma}(\theta^* - \pi) - \hat{\gamma}'(\theta^* - \pi)(\phi - \pi) + \frac{\hat{\gamma}''(\xi)}{2}(\phi - \pi)^2 \\ &= \hat{\gamma}(\theta^* - \pi) + \frac{\hat{\gamma}''(\xi)}{2}(\phi - \pi)^2.\end{aligned} \tag{5.10}$$

Again, by the mean value theorem, we know that there exists a ξ_1 between π, ϕ,

$$\cos\phi = -1 - \frac{\cos\xi_1}{6}(\phi - \pi)^2. \tag{5.11}$$

By substituting (5.10) and (5.11) into $2\hat{\gamma}(\theta^*) - Q(\phi, \theta^*)$, we have

$$\begin{aligned}2\hat{\gamma}(\theta^*) - Q(\phi, \theta^*) &= 2\hat{\gamma}(\theta^*) - \hat{\gamma}'(\theta^* - \pi) - \frac{\hat{\gamma}''(\xi)}{2}(\phi - \pi)^2 \\ &\quad + \hat{\gamma}(\theta^*) + \frac{\cos\xi_1}{6}\hat{\gamma}(\theta)(\phi - \pi)^2 + \hat{\gamma}(\theta^*)\sin\phi \\ &= \frac{1}{6}\left(\hat{\gamma}(\theta^*)\cos\xi_1 - 3\hat{\gamma}''(\xi)\right)(\phi - \pi)^2.\end{aligned} \tag{5.12}$$

Thus,

$$\begin{aligned}|2\hat{\gamma}(\theta^*) - Q(\phi, \theta^*)| &\le \frac{1}{6}\left(|\hat{\gamma}(\theta^*)\cos\xi_1| + 3|\hat{\gamma}''(\xi)|\right)|\phi - \pi|^2 \\ &\le \frac{2C}{3}|\phi - \pi|^2.\end{aligned} \tag{5.13}$$

Given that $|2\hat{\gamma}(\theta^*) + Q(\phi, \theta^*)| \le 5C$, we can deduce that

$$\begin{aligned}|4\hat{\gamma}^2(\theta^*) - Q^2(\phi, \theta^*)| &\le |2\hat{\gamma}(\theta^*) + Q(\phi, \theta^*)||2\hat{\gamma}(\theta^*) - Q(\phi, \theta^*)| \\ &\le \frac{10C^2}{3}|\phi - \pi|^2.\end{aligned} \tag{5.14}$$

Noting that for any $\phi \in U_\pi$, we have $|\sin\phi| = |\sin(\phi - \pi)| > \frac{2}{\pi}|\phi - \pi|$ since $\varepsilon \in (0, \frac{\pi}{2})$ and $|\phi - \pi| < \frac{\pi}{2}$. Therefore,

$$\begin{aligned}F_\alpha(\phi, \theta^*) &= 4\hat{\gamma}(\theta^*)\alpha\sin^2\phi + 4\hat{\gamma}^2(\theta^*) - Q^2(\phi, \theta^*) \\ &\ge \frac{16}{C\pi^2}\alpha|\phi - \pi|^2 - \frac{10C^2}{3}|\phi - \pi|^2 \\ &\ge \left[\frac{16}{C\pi^2}\alpha - \frac{10C^2}{3}\right]|\phi - \pi|^2, \ \forall\phi \in U_\pi.\end{aligned} \tag{5.15}$$

Therefore, there exists a positive constant $k_{U_\pi} := \frac{5\pi^2C^3}{24}$, such that for $\alpha > k_{U_\pi}$, we have $F_\alpha(\phi, \theta) \ge 0, \forall\phi \in U_\pi$. □

With the help of above two lemmas, Theorem 4.1 can now be proven:

Proof. (*Existence of the minimal stabilizing function*)

(i) For any $\sin\phi_0 \ne 0$, i.e. $\phi_0 \ne 0, \pi$, there exists an open neighborhood U_{ϕ_0} of ϕ_0 such that $\sin^2\phi$ has a strict positive lower bound in U_{ϕ_0}, i.e. there exists a constant $c > 0$ such that $\sin^2\phi \ge c > 0, \forall\phi \in U_{\phi_0}$, then we have

$$\begin{aligned}F_\alpha(\phi, \theta) &= 4\hat{\gamma}(\theta)\alpha\sin^2\phi + O(1) \\ &\ge 4c\hat{\gamma}(\theta)\alpha + O(1).\end{aligned} \tag{5.16}$$

Thus there positive exists a constant $k_{U_{\phi_0}} < +\infty$, for any $\alpha > k_{U_{\phi_0}}$, $F_\alpha(\phi, \theta) \ge 0, \forall\phi \in U_{\phi_0}$.

(ii) For $\phi_0 = 0$, by Lemma 5.1, there exists an open neighborhood $U_{\phi_0} := U_0$ of 0 and a positive constant $k_{U_{\phi_0}} := k_{U_0} < +\infty$ such that for any $\alpha > k_{U_{\phi_0}}$, $F_\alpha(\phi, \theta) \ge 0, \forall\phi \in U_{\phi_0}$.

(iii) For $\phi_0 = \pi$, by Lemma 5.2, there also exists an open neighborhood $U_{\phi_0} := U_\pi$ of π with a positive constant $k_{U_{\phi_0}} := k_{U_\pi} < +\infty$ such that for any $\alpha > k_{U_{\phi_0}}$, $F_\alpha(\phi, \theta) \ge 0, \forall\phi \in U_{\phi_0}$.

Since $2\pi\mathbb{T}$ is compact and $\{U_{\phi_0} : \phi_0 \in 2\pi\mathbb{T}\}$ forms an open cover of $2\pi\mathbb{T}$, by the open cover theorem, one can select a finite subcover $\{U_i\}_{i=1}^M \subset \{U_{\phi_0} : \phi_0 \in 2\pi\mathbb{T}\}$, then for $\alpha > \max_{1\le i\le M} k_{U_i}$, we have

$$F_\alpha(\phi, \theta) \ge 0, \qquad \forall\phi \in 2\pi\mathbb{T}. \tag{5.17}$$

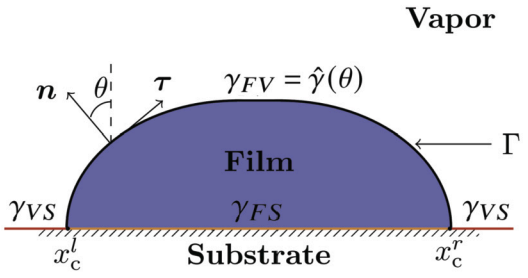

Fig. 2. An illustration of solid-state dewetting of a thin film on a flat rigid substrate in 2D, where $\gamma_{FV} = \hat{\gamma}(\theta), \gamma_{VS}, \gamma_{FS}$ represent surface energy densities of film/vapor, vapor/substrate and film/substrate interface, respectively, x_c^l, x_c^r are the left and right contact points.

Which implies $k_0(\theta) = \inf\left\{\alpha \geq 0 \mid P_\alpha(\phi,\theta) - Q(\phi,\theta) \geq 0,\ \forall \phi \in 2\pi\mathbb{T}\right\} < +\infty$. □

6. Extension to solid-state dewetting

In this section, we extend the conservative formulation (2.14) and its SPFEM (3.32) for a closed curve under anisotropic surface diffusion to solid-state dewetting in materials science [4,30,49].

6.1. Sharp interface model and a SPFEM

As shown in Fig. 2, the solid-state dewetting problem in 2D is described as evolution of an open curve $\Gamma(t) = \boldsymbol{X}(s,t) = (x(s,t), y(s,t))^T$ $(0 \leq s \leq L)$ under anisotropic surface diffusion and contact line migration. Here, s and t are the arc-length parameter and time, respectively, and $L := L(t) = |\Gamma(t)|$ represents the total length of $\Gamma(t)$. As it was derived in the literature [4,30,49], a dimensionless sharp-interface model for simulating solid-state dewetting of thin films with weakly anisotropic surface energy can be formulated as: $\boldsymbol{X}(s,t)$ satisfying anisotropic surface diffusion (1.1)-(1.2) with following boundary conditions

1. contact point condition

$$y(0,t) = 0, \qquad y(L,t) = 0, \qquad t \geq 0; \tag{6.1}$$

2. relaxed contact angle condition

$$\frac{\mathrm{d}x_c^l(t)}{\mathrm{d}t} = \eta f(\theta_d^l;\sigma), \qquad \frac{\mathrm{d}x_c^r(t)}{\mathrm{d}t} = -\eta f(\theta_d^r;\sigma), \qquad t \geq 0; \tag{6.2}$$

3. zero-mass flux condition

$$\partial_s \mu(0,t) = 0, \qquad \partial_s \mu(L,t) = 0, \qquad t \geq 0; \tag{6.3}$$

where $x_c^l(t) = x(0,t) \leq x_c^r(t) = x(L,t)$ are the left and right contact points, $\theta_d^l := \theta_d^l(t), \theta_d^r := \theta_d^r(t)$ are the contact angles at each contact points, respectively. $f(\theta;\sigma)$ is defined as

$$f(\theta;\sigma) := \hat{\gamma}(\theta)\cos\theta - \hat{\gamma}'(\theta)\sin\theta - \sigma, \qquad \theta \in 2\pi\mathbb{T}. \tag{6.4}$$

with $\sigma := \cos\theta_Y = \frac{\gamma_{VS}-\gamma_{FS}}{\gamma_{FV}}$ and θ_Y be the isotropic Young contact angle. $0 < \eta < +\infty$ denotes the contact line mobility [4,30,49].

Introduce the finite element spaces

$$\mathbb{K}_0^h := \left\{u^h \in \mathbb{K}^h \mid u^h(0) = u^h(1) = 0\right\}, \qquad \mathbb{X}^h := \mathbb{K}^h \times \mathbb{K}_0^h. \tag{6.5}$$

Similarly to the derivations in [35,36], a structure-preserving discretization of the SPFEM for solid-state dewetting can be stated as follows: Suppose the initial approximation $\Gamma^0(\cdot) \in \mathbb{X}^h$ is given by $\boldsymbol{X}^0(\rho_j) = \boldsymbol{X}_0(\rho_j), \forall 0 \leq j \leq N$. For any $m = 0, 1, 2, \ldots$, find the solution $(\boldsymbol{X}^{m+1}(\cdot) = (x^{m+1}(\cdot), y^{m+1}(\cdot))^T, \mu^{m+1}(\cdot)) \in \mathbb{X}^h \times \mathbb{K}^h$, such that

$$\left(\boldsymbol{n}^{m+\frac{1}{2}} \cdot \frac{\boldsymbol{X}^{m+1} - \boldsymbol{X}^m}{\tau}, \varphi^h\right)_{\Gamma^m}^h + \left(\partial_s \mu^{m+1}, \partial_s \varphi^h\right)_{\Gamma^m}^h = 0, \qquad \forall \varphi^h \in \mathbb{K}^h, \tag{6.6a}$$

$$\begin{aligned}\left(\mu^{m+1}\boldsymbol{n}^{m+\frac{1}{2}}, \boldsymbol{\omega}^h\right)_{\Gamma^m}^h - \left(\hat{\boldsymbol{G}}_k(\theta^m)\partial_s \boldsymbol{X}^m, \partial_s \boldsymbol{\omega}^h\right)_{\Gamma^m}^h - \frac{1}{\eta}\left[\frac{x_l^{m+1} - x_l^m}{\tau}\omega_1^h(0) + \frac{x_r^{m+1} - x_r^m}{\tau}\omega_1^h(1)\right] \\ + \sigma\left[\omega_1^h(1) - \omega_1^h(0)\right] = 0, \qquad \forall \boldsymbol{\omega}^h = (\omega_1^h, \omega_2^h) \in \mathbb{X}^h,\end{aligned} \tag{6.6b}$$

satisfying $x_l^{m+1} = x^{m+1}(0) \leq x_r^{m+1} = x^{m+1}(1)$. The definition of $\hat{\boldsymbol{G}}_k(\theta^m)$ is similar to (3.34).

Denote the area A_o^m enclosed by the open polygonal curve $\Gamma(t)$ and the substrate and the total surface energy W_o^m as

$$A_o^m := \frac{1}{2}\sum_{j=1}^{N}\left(x^m(\rho_j)-x^m(\rho_{j-1})\right)\left(y^m(\rho_j)+y^m(\rho_{j-1})\right), \tag{6.7a}$$

$$W_o^m := \sum_{j=1}^{N}|\boldsymbol{h}_j^m|\hat{\gamma}(\theta_j^m)-\sigma\left(x_r^m-x_l^m\right). \tag{6.7b}$$

Then for the SPFEM (6.6), we have following result.

Theorem 6.1 *(Structure-preserving). For any $\hat{\gamma}(\theta)$ satisfying (3.36), the SPFEM (6.6) is area conservative and unconditional energy dissipative with sufficiently large $k(\theta)$, i.e.*

$$A_o^{m+1}=A_o^m=\cdots=A_o^0, \qquad W_o^{m+1}\le W_o^m\le\cdots\le W_o^0, \qquad \forall m\ge 0. \tag{6.8}$$

The proof is similar to Theorem 3.1 or [35, Proposition 5.4], [10, Theorem 3.2]. We omit the details here for brevity.

Remark 6.1. Due to the local energy estimate (4.2) being only dependent on $\hat{\gamma}(\theta)$, all results concerning the energy dissipation of the SPFEM (3.32) on evolutions of closed curves can be extended to the SPFEM (6.6) on evolutions of open curves in solid-state dewetting, including Remark 3.4 – 3.6.

7. Numerical results

In this section, we report numerical experiments for the proposed SPFEM (3.32) and (6.6) for time evolutions of closed curves and open curves, respectively. Extensive results are provided to illustrate their efficiency, accuracy, area conservation and unconditional energy stability.

In the numerical tests, following typical anisotropic surface energies are considered in the simulations:

- Case I: $\hat{\gamma}(\theta)=1+\beta\cos 3\theta$ with $|\beta|<1$. It is weakly anisotropic when $|\beta|<\frac{1}{8}$ and strongly anisotropic otherwise;
- Case II: $\hat{\gamma}(\theta)=\sqrt{1+b\cos^2\theta}$ with $b>-1$.

To compute the minimal stabilizing function $k_0(\theta)$, we solve the optimization problem (4.4) for 20 uniformly distributed points $\theta_j=-\pi+\frac{j\pi}{10}$, $\forall 1\le j\le 20$ in $[-\pi,\pi]$ to get $k_0(\theta_j)$ and do linear interpolation for the intermediate points $\theta\in(\frac{j\pi}{10},\frac{(j+1)\pi}{10})$, i.e. set $k_0(\theta)=(1-\lambda)k_0(\theta_j)+\lambda k_0(\theta_{j+1})$ where $\lambda=\frac{10}{\pi}(\theta-\frac{j\pi}{10})$.

To verify the quadratic convergence rate in space and linear convergence rate in time, the time step τ is always chosen as $\tau=16h^2$ except it is stated otherwise. The manifold distance [36,53]

$$M(\Gamma_1,\Gamma_2) := 2|\Omega_1\cup\Omega_2|-|\Omega_1|-|\Omega_2|, \tag{7.1}$$

is employed to measure the distance between two closed curves Γ_1,Γ_2, where Ω_1,Ω_2 are the regions enclosed by Γ_1,Γ_2 and $|\Omega|$ represents the area of $|\Omega|$. Suppose Γ^m is the numerical approximation of $\Gamma^h(t=t_m:=m\tau)$, thus the numerical error is defined as

$$e^h(t)\Big|_{t=t_m} := M(\Gamma^m,\Gamma(t=t_m)). \tag{7.2}$$

In the Newton's iteration, the tolerance value is set to be $\mathrm{tol}=10^{-12}$.

To test the mesh quality, the energy stability and area conservation numerically, we introduce the following indicators: the weighted mesh ratio

$$R_\gamma^h(t) := \frac{\max\limits_{1\le j\le N}\hat{\gamma}(\theta_j)|\boldsymbol{h}_j|}{\min\limits_{1\le j\le N}\hat{\gamma}(\theta_j)|\boldsymbol{h}_j|}, \tag{7.3}$$

the normalized area loss and the normalized energy for closed curves:

$$\frac{\Delta A_c^h(t)}{A_c^h(0)}\Big|_{t=t_m} := \frac{A_c^m-A_c^0}{A_c^0}, \qquad \frac{W_c^h(t)}{W_c^h(0)}\Big|_{t=t_m} := \frac{W_c^m}{W_c^0}, \tag{7.4}$$

and for open curves:

$$\frac{\Delta A_o^h(t)}{A_o^h(0)}\Big|_{t=t_m} := \frac{A_o^m-A_o^0}{A_o^0}, \qquad \frac{W_o^h(t)}{W_o^h(0)}\Big|_{t=t_m} := \frac{W_o^m}{W_o^0}. \tag{7.5}$$

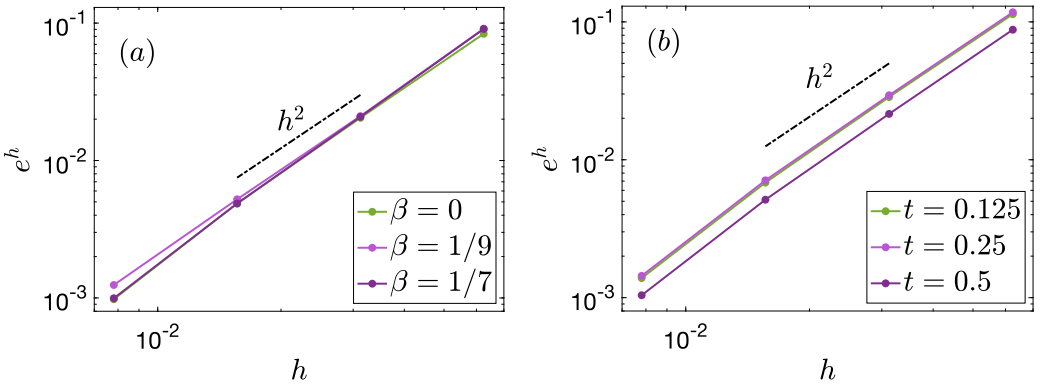

Fig. 3. Convergence rates of the SPFEM (3.32) with $k(\theta) = k_0(\theta)$ for: (a) anisotropy in Case I at $t = 0.5$ with different β; and (b) anisotropy in Case II with $b = -0.8$ at different times $t = 0.125, 0.25, 0.5$. (For interpretation of the colors in the figure(s), the reader is referred to the web version of this article.)

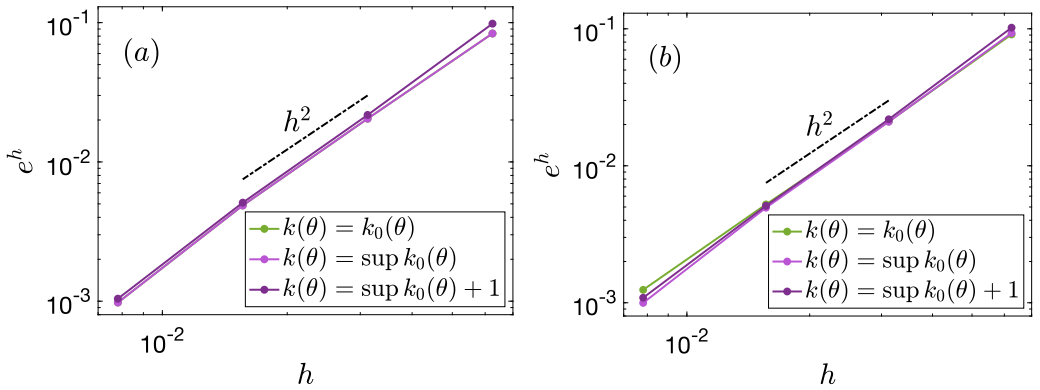

Fig. 4. Convergence rates of the SPFEM (3.32) for Case I at $t = 0.5$ with different $k(\theta)$: (a) $\beta = 0$; and (b) $\beta = 1/9$.

In the following numerical tests, the initial shapes are chosen as a complete and a half ellipse with major axis 4 and minor axis 1 for closed curves and open curves, respectively, unless stated otherwise. The exact solution $\Gamma(t)$ is approximated by choosing $k(\theta) = k_0(\theta)$ with a small mesh size $h_e = 2^{-8}$ and a time step $\tau_e = 2^{-12}$ in (3.32). For solid-state dewetting problems, we always choose the contact line mobility $\eta = 100$.

7.1. Results for closed curves

Fig. 3 plots the convergence rates of the proposed SPFEM (3.32) for: (a) the 3-fold anisotropy $\hat{\gamma}(\theta) = 1 + \beta\cos 3\theta$ with different anisotropic strengths β under a fixed time $t = 0.5$; (b) the ellipsoidal anisotropy $\hat{\gamma}(\theta) = \sqrt{1 - 0.8\cos^2\theta}$ at different times. It clearly demonstrates that the second-order spatial convergence remains consistent regardless of anisotropies and computational times, suggesting a high level of robustness in the convergence rate.

Fig. 4 displays the convergence rates of the proposed SPFEM (3.32) for Case I with different values of $k(\theta)$. Fig. 4 (a) corresponds to $\beta = 0$, and Fig. 4 (b) corresponds to $\beta = \frac{1}{9}$. It can be observed that varying the pre-allocated $k(\theta)$ does not affect the convergence rate.

Fig. 5 exhibits that the weighted mesh ratio R_γ^h converges to constants as $t \to +\infty$. This suggests an asymptotic quasi-uniform mesh distribution of the proposed SPFEM (3.32).

The time evolution of the normalized area loss $\frac{\Delta A_c^h(t)}{A_c^h(0)}$, the number of the Newton's iteration with $h = 2^{-7}, \tau = 2^{-10}$ are given in Fig. 6. And the normalized energy $\frac{W_c^h(t)}{W_c^h(t)}$ with different h are summarized in Fig. 7.

The observation from Fig. 6 – Fig. 7 reveals that:

1. The normalized area loss is at 10^{-16}, aligns closely with the order of the round-off error (cf. Fig. 6). This observation affirms the practical preservation of area in simulations.
2. The numbers of the Newton's iteration are initially 3 or 4, and quickly descend to 2 (cf. Fig. 6). This discovery indicates that the proposed SPFEM (3.32) can be solved with high efficiency, requiring only a few iterations.
3. The normalized energy is monotonically decreasing when $\hat{\gamma}(\theta)$ satisfies the energy stable conditions (3.36) in Definition 3.1 (cf. Fig. 7). Results in Fig. 7 (a) shows that the proposed SPFEM (3.32) still preserves good energy stability properties when β takes

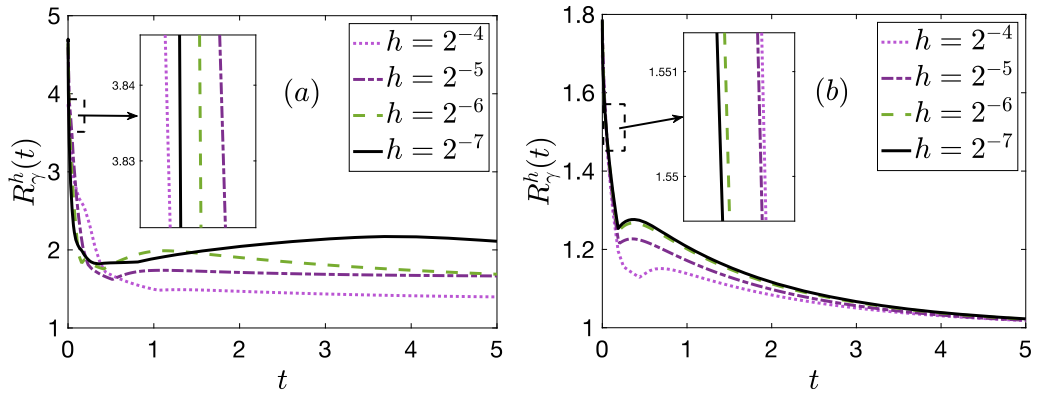

Fig. 5. Weighted mesh ratio of the SPFEM (3.32) with $k(\theta) = k_0(\theta)$ for: (a) anisotropy in Case I with $\beta = \frac{1}{9}$; and (b) anisotropy in Case II with $b = -0.8$.

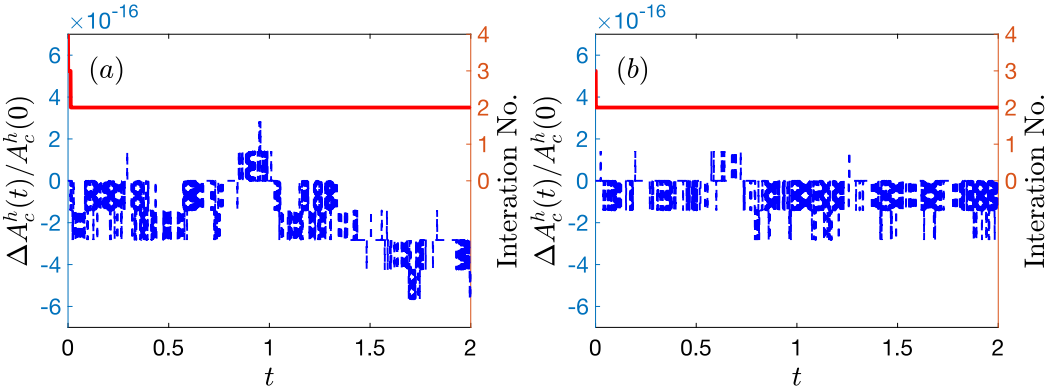

Fig. 6. Normalized area loss (blue dashed line) and iteration number (red line) of the SPFEM (3.32) with $k(\theta) = k_0(\theta)$ and $h = 2^{-7}, \tau = 2^{-10}$ for: (a) anisotropy in Case I with $\beta = \frac{1}{2}$; and (b) anisotropy in Case II with $b = -0.8$.

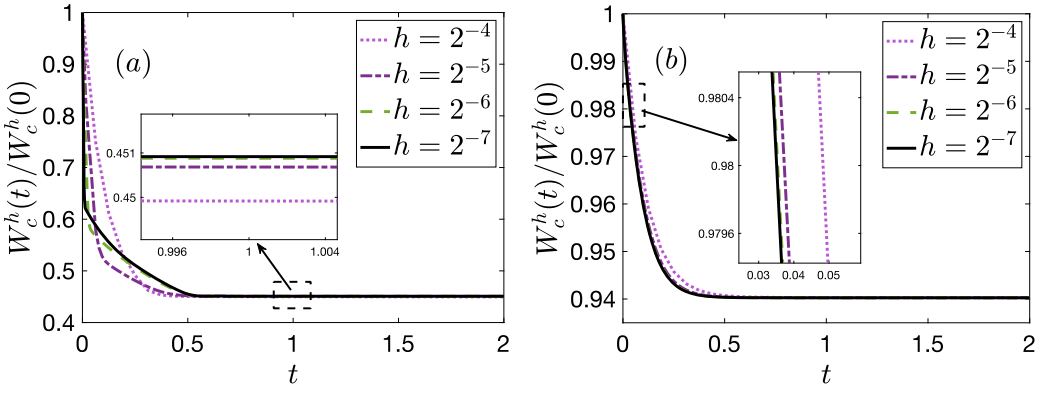

Fig. 7. Normalized energy of the SPFEM (3.32) with $k(\theta) = k_0(\theta)$ for: (a) anisotropy in Case I with $\beta = \frac{1}{2}$; and (b) anisotropy in Case II with $b = -0.8$.

its maximum value of $1/2$ in Remark 3.4. And results in Fig. 7 (b) indicate that, unlike the ES-PFEM in [36], the SPFEM remains unconditionally energy stable when $b < -1/2$ as stated in Remark 3.5.

7.2. Results for open curves in solid-state dewetting

Fig. 8 plots the computation errors of the proposed SPFEM (6.6) for: (a) the 3-fold anisotropy $\hat{\gamma}(\theta) = 1 + \beta\cos 3\theta$ with different anisotropic strengths β under a fixed time $t = 0.5$; (b) the ellipsoidal anisotropy $\hat{\gamma}(\theta) = \sqrt{1 + 2\cos^2\theta}$ at different times. The results verify the quadratic convergence rate for the proposed SPFEM (6.6).

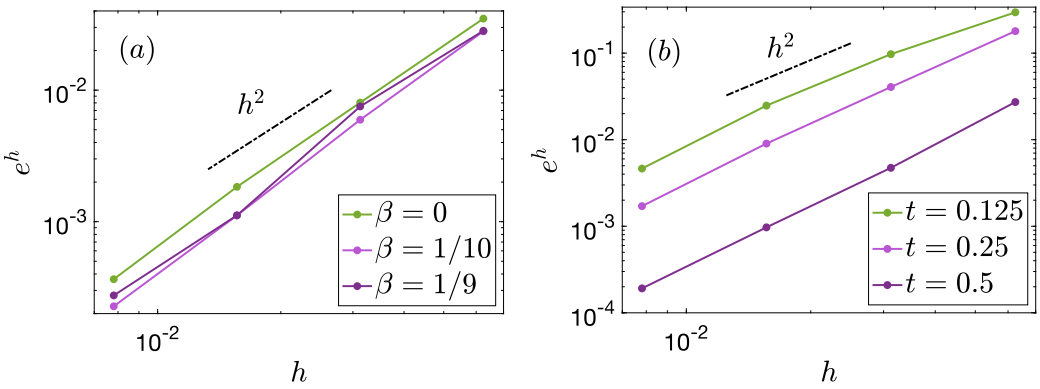

Fig. 8. Convergence rates of the SPFEM (3.32) with $k(\theta) = k_0(\theta)$ and $\sigma = -\frac{\sqrt{2}}{2}$ for: (a) anisotropy in Case I at $t = 0.5$ with different β; and (b) anisotropy in Case II with $b = 2$ at different times $t = 0.125, 0.25, 0.5$.

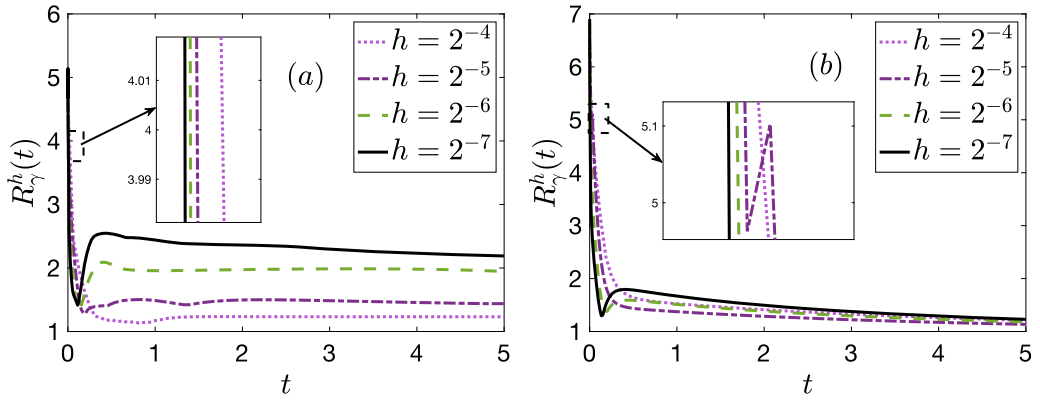

Fig. 9. Weighted mesh ratio of the SPFEM (3.32) with $k(\theta) = k_0(\theta)$ and $\sigma = -\frac{\sqrt{2}}{2}$ for: (a) anisotropy in Case I with $\beta = \frac{1}{9}$; (b) anisotropy in Case II with $b = 2$.

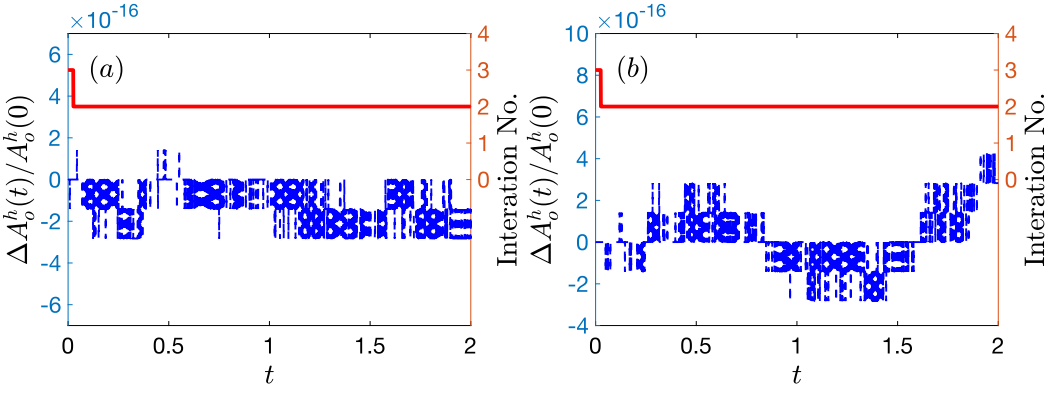

Fig. 10. Normalized area loss (blue dashed line) and iteration number (red line) of the SPFEM (3.32) with $k(\theta) = k_0(\theta)$, $\sigma = -\frac{\sqrt{2}}{2}$ and $h = 2^{-7}, \tau = 2^{-10}$ for: (a) anisotropy in Case I with $\beta = \frac{1}{9}$; and (b) anisotropy in Case II with $b = 2$.

In Fig. 9, the weighted mesh ratios R_γ^h tend to constants as $t \to +\infty$, showing that the SPFEM (6.6) still possesses the asymptotic quasi-uniform distribution.

Time evolutions of the normalized area loss $\frac{\Delta A_o^h(t)}{A_o^h(0)}$, the number of the Newton's iteration with $h = 2^{-7}, \tau = 2^{-10}$ are presented in Fig. 10. And the normalized energy $\frac{W_o^h(t)}{W_o^h(t)}$ with different h are illustrated in Fig. 11.

It can be observed from Fig. 7 – Fig. 10 that:

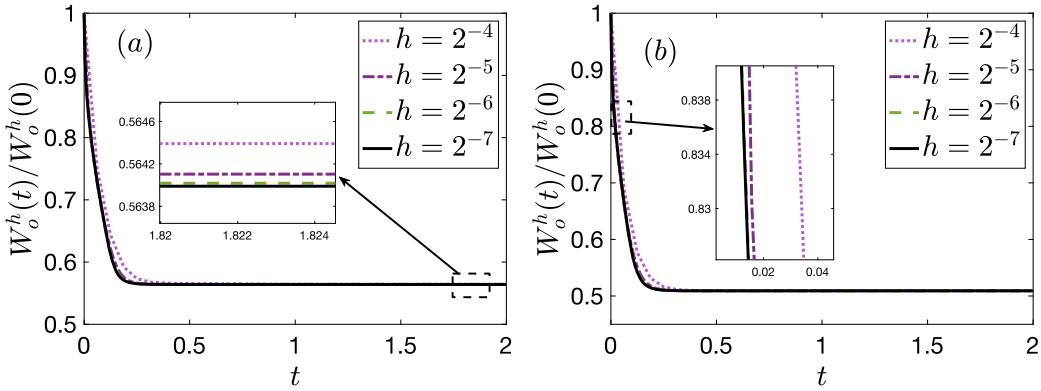

Fig. 11. Normalized energy of the SPFEM (3.32) with $k(\theta) = k_0(\theta)$ and $\sigma = -\frac{\sqrt{2}}{2}$ for: (a) anisotropy in Case I with $\beta = \frac{1}{9}$; and (b) anisotropy in Case II with $b = 2$.

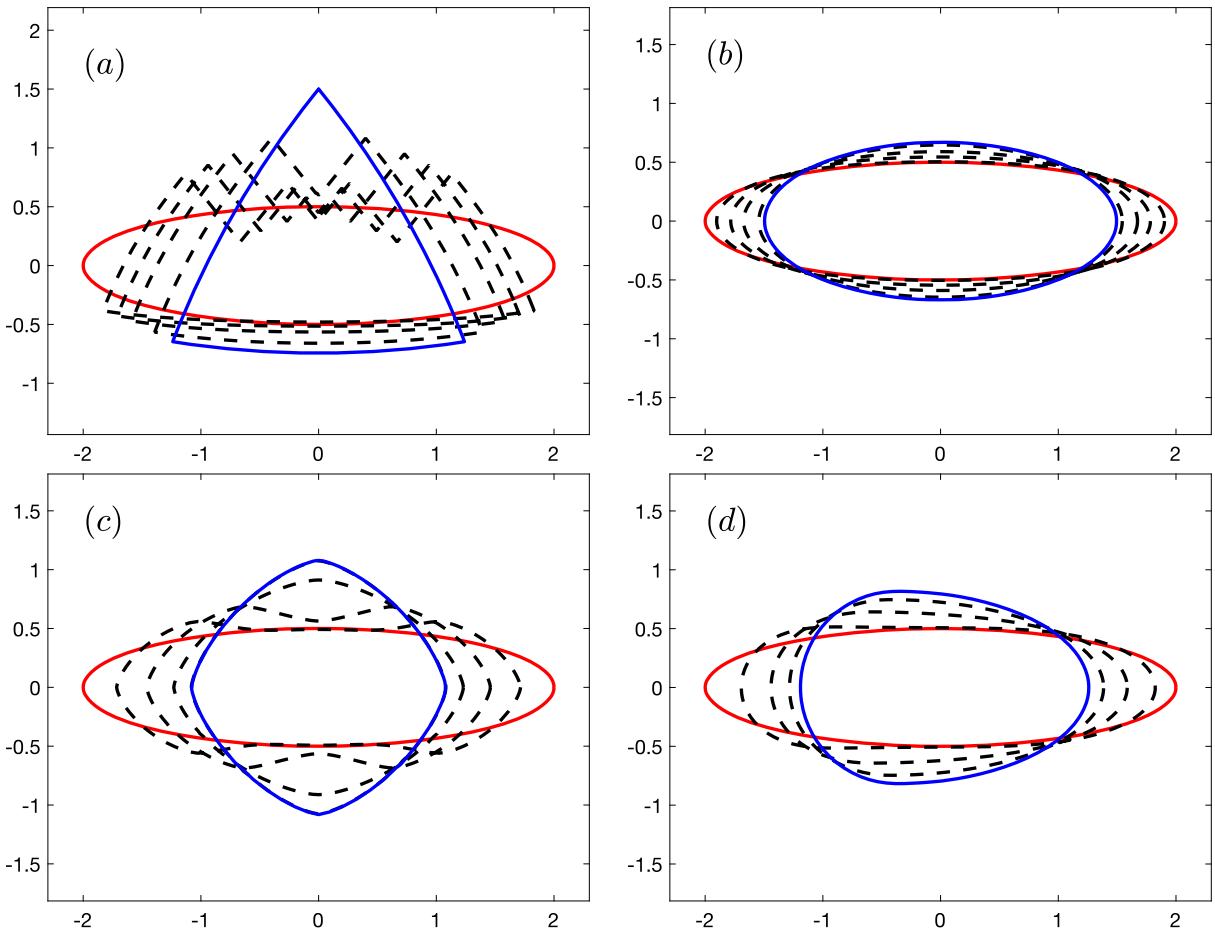

Fig. 12. Morphological evolutions of an ellipse with major axis 4 and minor axis 1 under anisotropic surface diffusion with different surface energies: (a) anisotropy in Case I with $\beta = \frac{1}{2}$; (b) anisotropy in Case II with $b = -0.8$; (c) $\hat{\gamma}(\theta) = 1 + \frac{1}{16}\cos 4\theta$; (d) $\hat{\gamma}(\theta) = \sqrt{\left(\frac{5}{2} + \frac{3}{2}\mathrm{sgn}(n_1)\right) n_1^2 + n_2^2}$ with $\boldsymbol{n} = (n_1, n_2)^T = (-\sin\theta, \cos\theta)^T$. The red and blue lines represent the initial shape and the numerical equilibrium, respectively; and the black dashed lines represent the intermediate curves. The mesh size and the time step are taken as $h = 2^{-7}, \tau = 2^{-10}$.

1. The normalized area loss is about 10^{-16} at the same order of the round-off error (cf. Fig. 10), verifying that the area is conserved up to the machine precision.
2. The numbers of the Newton's iteration are initially 3 and finally 2 (cf. Fig. 10). This finding suggests that, despite the fully-implicit nature of the proposed SPFEM (6.6), it can be solved very efficiently.

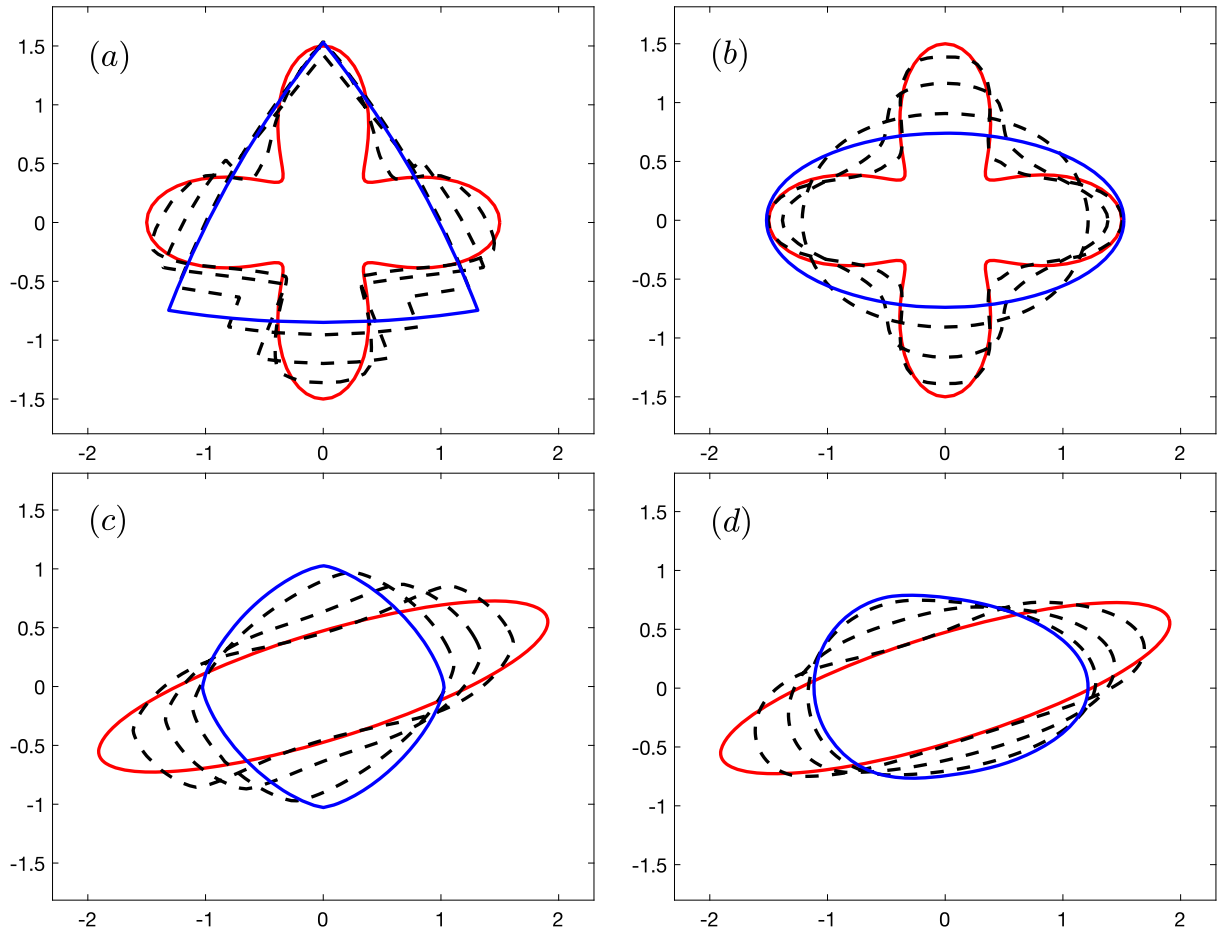

Fig. 13. Morphological evolutions of a four-fold star shape curve and a rotated ellipse under anisotropic surface diffusion with different surface energies: (a) anisotropy in Case I with $\beta = \frac{1}{2}$; (b) anisotropy in Case II with $b = -0.8$; (c) $\hat{\gamma}(\theta) = 1 + \frac{1}{16}\cos 4\theta$; (d) $\hat{\gamma}(\theta) = \sqrt{\left(\frac{5}{2} + \frac{3}{2}\mathrm{sgn}(n_1)\right) n_1^2 + n_2^2}$ with $\boldsymbol{n} = (n_1, n_2)^T = (-\sin\theta, \cos\theta)^T$. The red and blue lines represent the initial shape and the numerical equilibrium, respectively; and the black dashed lines represent the intermediate curves. The mesh size and the time step are taken as $h = 2^{-7}, \tau = 2^{-10}$.

3. The normalized energy is monotonically decreasing when $\hat{\gamma}(\theta)$ satisfying (3.36) (cf. Fig. 11). In contrast to the ES-PFEM in [36], the proposed SPFEM (6.6) still guarantees the energy dissipation when $\beta < \frac{1}{10}$ in Case I and $b > 1$ in Case II, as asserted by Remark 3.4 and Remark 3.5.

7.3. Application for morphological evolutions

Finally we apply the proposed SPFEMs (3.32) and (6.6) to simulate the morphological evolutions under the anisotropic surface diffusion. Results for both closed curves and open curves in solid-state dewetting problems are provided.

The morphological evolutions from the initial shapes to their numerical equilibriums are presented in Fig. 12 – Fig. 14. For closed curve cases, the initial shape is an ellipse with major axis 4 and minor axis 1, while for open curve cases, it is an open 4×1 rectangle.

Fig. 12 plots the morphological evolutions of an ellipse with major axis 4 and minor axis 1 under anisotropic surface diffusion with four different surface energies: (a) anisotropy in Case I with $\beta = \frac{1}{2}$, which attends the maximum value in Remark 3.4; (b) anisotropy in Case II with $b = -0.8$; (c) the 4-fold anisotropy $\hat{\gamma}(\theta) = 1 + \frac{1}{16}\cos 4\theta$ [4]; and (d) $\hat{\gamma}(\theta) = \sqrt{\left(\frac{5}{2} + \frac{3}{2}\mathrm{sgn}(n_1)\right) n_1^2 + n_2^2}$ with $\boldsymbol{n} = (n_1, n_2)^T = (-\sin\theta, \cos\theta)^T$ [20].

Results in Fig. 12 (b) and Fig. 12 (c) show that, compared to the ES-PFEM in [36], the proposed SPFEM (3.32) demonstrates a better performance over a broader range of parameters during evolutions. Fig. 12 (d) indicates that the SPFEM (3.32) also works well for a globally C^1 and piecewise C^2 anisotropy.

And Fig. 13 illustrates the morphological evolutions under anisotropic surface diffusion with different surface energies for a four-fold star shape curve

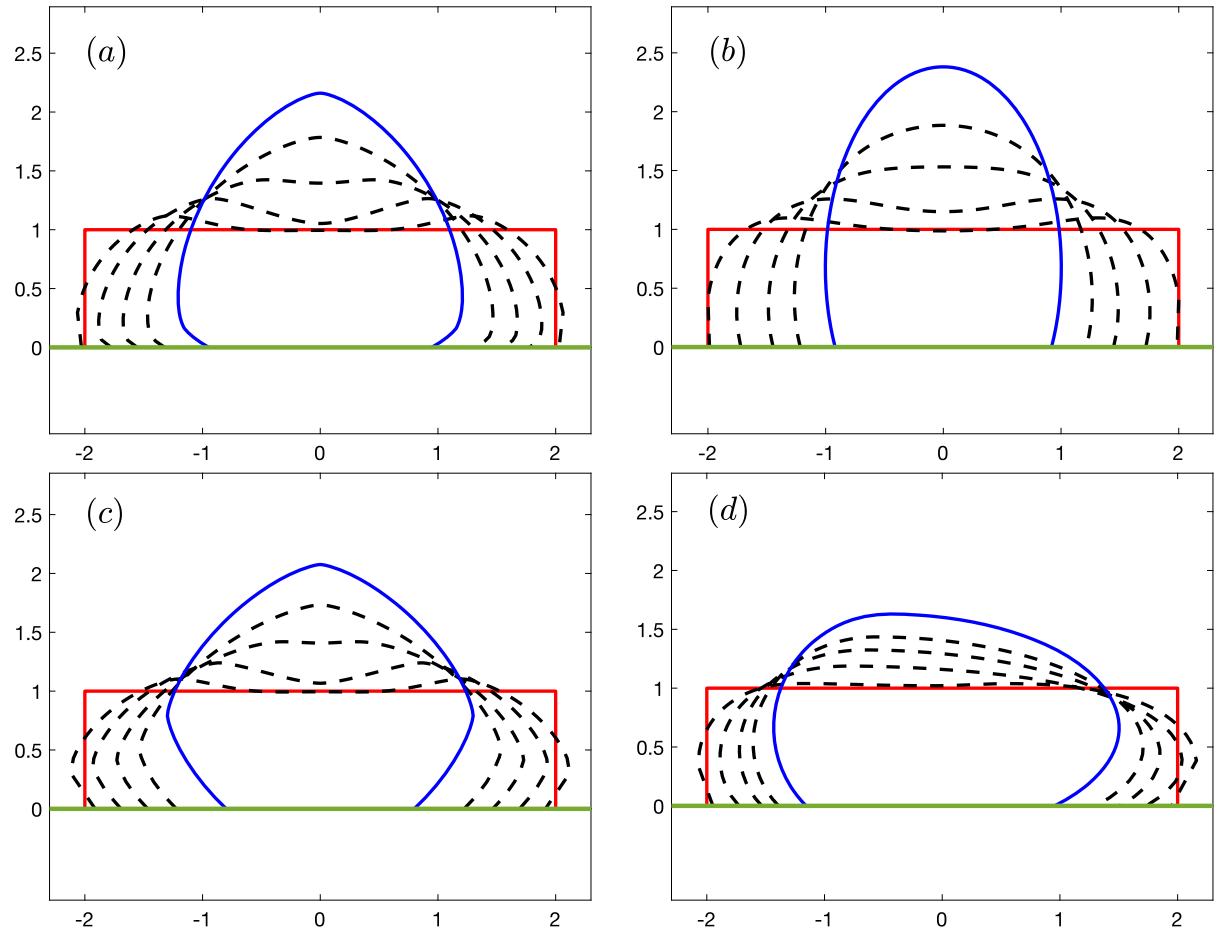

Fig. 14. Morphological evolutions of an open 4×1 rectangle under anisotropic surface diffusion with different surface energies: (a) anisotropy in Case I with $\beta=\frac{1}{9}$; (b) anisotropy in Case II with $b=2$; (c) $\hat{\gamma}(\theta)=1+\frac{1}{16}\cos 4\theta$; (d) $\hat{\gamma}(\theta)=\sqrt{\left(\frac{5}{2}+\frac{3}{2}\mathrm{sgn}(n_1)\right)n_1^2+n_2^2}$ with $\boldsymbol{n}=(n_1,n_2)^T=(-\sin\theta,\cos\theta)^T$. The red and blue lines represent the initial shape and the numerical equilibrium, respectively; and the black dashed lines represent the intermediate curves. The parameters are chosen as $\sigma=-\frac{\sqrt{2}}{2}, h=2^{-7}, \tau=2^{-10}$.

$$\begin{cases} x=(1+0.5\cos 4\theta)\cos\theta, \\ y=(1+0.5\cos 4\theta)\sin\theta, \end{cases} \quad \theta\in 2\pi\mathbb{T}, \tag{7.6}$$

and an ellipse (with major axis 4 and minor axis 1) rotated counterclockwise by $\frac{\pi}{10}$.

In Fig. 14, we display the morphological evolutions from an open 4×1 rectangular curve to their equilibriums shapes with different surface energies: (a) anisotropy in Case I with $\beta=\frac{1}{9}$; (b) anisotropy in Case II with $b=2$; (c) the 4-fold anisotropy $\hat{\gamma}(\theta)=1+\frac{1}{16}\cos 4\theta$; (d) $\hat{\gamma}(\theta)=\sqrt{\left(\frac{5}{2}+\frac{3}{2}\mathrm{sgn}(n_1)\right)n_1^2+n_2^2}$ with $\boldsymbol{n}=(n_1,n_2)^T=(-\sin\theta,\cos\theta)^T$.

Similar to the closed curve cases, the SPFEM (6.6) extends the choices in surface energies for simulating solid-state dewetting (cf. Fig. 14 (a) – Fig. 14 (c)). And Fig. 14 (d) illustrates that our method also performs effectively for $\hat{\gamma}(\theta)$ with lower regularity.

8. Conclusions

We propose a structure-preserving stabilized parametric finite element method (SPFEM) for the anisotropic surface diffusion. This method is subject to mild conditions on $\hat{\gamma}(\theta)$, and works effectively for closed curves and open curves with contact line migration in solid-state dewetting. By introducing a new stabilized surface energy matrix, we obtain a conservative form and its weak formulation for anisotropic surface diffusion. Based on this weak formulation, a novel SPFEM is proposed by utilizing the PFEM for spatial discretization and the implicit-explicit Euler method for temporal discretization. To analyze the unconditional energy stability, we extend the framework proposed by Bao and Li to the $\hat{\gamma}(\theta)$ formulation. This approach starts by defining the minimal stabilizing function, proving its existence, results in a local energy estimate, and subsequently establishes unconditional energy stability. Due to the very mild requirements on the surface energy $\hat{\gamma}(\theta)$, the methods are able to simulate over a broader range of anisotropies for

both closed curves and open curves. Moreover, the SPFEMs are applicable for the globally C^1 and piecewise C^2 anisotropy as well, which is a capability not possessed by other PFEMs.

CRediT authorship contribution statement

Yulin Zhang: Writing – original draft, Software, Methodology, Investigation, Conceptualization. **Yifei Li:** Writing – review & editing, Supervision, Project administration. **Wenjun Ying:** Writing – review & editing, Supervision.

Declaration of competing interest

The authors declare that they have no known competing financial interests or personal relationships that could have appeared to influence the work reported in this paper.

Acknowledgement

We would like to especially thank Professor Weizhu Bao for his valuable suggestions and comments. The work of Zhang was partially supported by the State Scholarship Fund administered by the Chinese Scholar Council (CSC) (No. 202306230346), and the Zhiyuan Honors Program for Graduate Students of Shanghai Jiao Tong University (No.021071910051). The work of Li was funded by the Ministry of Education of Singapore under its AcRF Tier 2 funding MOE-T2EP20122-0002 (A-8000962-00-00). Part of the work was done when the authors were visiting the Institute of Mathematical Science at the National University of Singapore in 2024. W. Ying is supported by the Shanghai Science and Technology Innovation Action Plan in Basic Research Area (Project No. 22JC1401700), the National Natural Science Foundation of China in the Division of Mathematical Sciences (Project No. 12471342). It is also partially supported by the National Key R&D Program of China (Project No. 2020YFA0712000) and the fundamental research funds for the central universities.

Data availability

Data will be made available on request.

References

[1] E. Bänsch, P. Morin, R. Nochetto, A finite element method for surface diffusion: the parametric case, J. Comput. Phys. 203 (2005) 321–343.
[2] W. Bao, H. Garcke, R. Nürnberg, Q. Zhao, Volume-preserving parametric finite element methods for axisymmetric geometric evolution equations, J. Comput. Phys. 460 (2022) 111180.
[3] W. Bao, H. Garcke, R. Nürnberg, Q. Zhao, A structure-preserving finite element approximation of surface diffusion for curve networks and surface clusters, Numer. Methods Partial Differ. Equ. 39 (2023) 759–794.
[4] W. Bao, W. Jiang, Y. Wang, Q. Zhao, A parametric finite element method for solid-state dewetting problems with anisotropic surface energies, J. Comput. Phys. 330 (2017) 380–400.
[5] W. Bao, W. Jiang, Y. Li, A symmetrized parametric finite element method for anisotropic surface diffusion of closed curves, SIAM J. Numer. Anal. 61 (2023) 617–641.
[6] W. Bao, W. Jiang, D. Srolovitz, Y. Wang, Stable equilibria of anisotropic particles on substrates: a generalized Winterbottom construction, SIAM J. Appl. Math. 77 (2017) 2093–2118.
[7] W. Bao, Y. Li, A structure-preserving parametric finite element method for geometric flows with anisotropic surface energy, Numer. Math. 156 (2024) 609–639.
[8] W. Bao, Y. Li, A symmetrized parametric finite element method for anisotropic surface diffusion in three dimensions, SIAM J. Sci. Comput. 45 (2023) A1438–A1461.
[9] W. Bao, Y. Li, A unified structure-preserving parametric finite element method for anisotropic surface diffusion, Preprint, arXiv:2401.00207, 2023.
[10] W. Bao, Q. Zhao, An energy-stable parametric finite element method for simulating solid-state dewetting problems in three dimensions, J. Comput. Math. 41 (2023) 771–796.
[11] W. Bao, Q. Zhao, A structure-preserving parametric finite element method for surface diffusion, SIAM J. Numer. Anal. 59 (2021) 2775–2799.
[12] J. Barrett, H. Garcke, R. Nürnberg, A parametric finite element method for fourth order geometric evolution equations, J. Comput. Phys. 222 (2007) 441–467.
[13] J. Barrett, H. Garcke, R. Nürnberg, On the variational approximation of combined second and fourth order geometric evolution equations, SIAM J. Sci. Comput. 29 (2007) 1006–1041.
[14] J. Barrett, H. Garcke, R. Nürnberg, Numerical approximation of anisotropic geometric evolution equations in the plane, IMA J. Numer. Anal. 28 (2008) 292–330.
[15] J. Barrett, H. Garcke, R. Nürnberg, On the parametric finite element approximation of evolving hypersurfaces in R3, J. Comput. Phys. 227 (2008) 4281–4307.
[16] J. Barrett, H. Garcke, R. Nürnberg, A variational formulation of anisotropic geometric evolution equations in higher dimensions, Numer. Math. 109 (2008) 1–44.
[17] J. Barrett, H. Garcke, R. Nürnberg, Parametric finite element approximations of curvature-driven interface evolutions, Handb. Numer. Anal. 21 (2020) 275–423.
[18] J. Cahn, J. Taylor, Overview no. 113 surface motion by surface diffusion, Acta Metall. Mater. 42 (1994) 1045–1063.
[19] L. Chen, J. Shen, Applications of semi-implicit Fourier-spectral method to phase field equations, Comput. Phys. Commun. 108 (1998) 147–159.
[20] K. Deckelnick, G. Dziuk, C. Elliott, Computation of geometric partial differential equations and mean curvature flow, Acta Numer. 14 (2005) 139–232.
[21] P. Du, M. Khenner, H. Wong, A tangent-plane marker-particle method for the computation of three-dimensional solid surfaces evolving by surface diffusion on a substrate, J. Comput. Phys. 229 (2010) 813–827.
[22] Q. Du, X. Feng, The phase field method for geometric moving interfaces and their numerical approximations, Handb. Numer. Anal. 21 (2020) 425–508.
[23] I. Fonseca, A. Pratelli, B. Zwicknagl, Shapes of epitaxially grown quantum dots, Arch. Ration. Mech. Anal. 214 (2014) 359–401.
[24] H. Garcke, P. Knopf, R. Nürnberg, Q. Zhao, A diffuse-interface approach for solid-state dewetting with anisotropic surface energies, J. Nonlinear Sci. 33 (2023) 34.
[25] G. Gilmer, P. Bennema, Simulation of crystal growth with surface diffusion, J. Appl. Phys. 43 (1972) 1347–1360.
[26] R. Gomer, Diffusion of adsorbates on metal surfaces, Rep. Prog. Phys. 53 (1990) 917.
[27] F. Guillén-González, G. Tierra, On linear schemes for a Cahn–Hilliard diffuse interface model, J. Comput. Phys. 234 (2013) 140–171.

[28] M. Gurtin, M. Jabbour, Interface evolution in three dimensions with curvature-dependent energy and surface diffusion: interface-controlled evolution, phase transitions, epitaxial growth of elastic films, Arch. Ration. Mech. Anal. 163 (2002) 171–208.
[29] W. Jiang, W. Bao, C. Thompson, D. Srolovitz, Phase field approach for simulating solid-state dewetting problems, Acta Mater. 60 (2012) 5578–5592.
[30] W. Jiang, Y. Wang, Q. Zhao, D. Srolovitz, W. Bao, Solid-state dewetting and island morphologies in strongly anisotropic materials, Scr. Mater. 115 (2016) 123–127.
[31] W. Jiang, Y. Wang, D. Srolovitz, W. Bao, Solid-state dewetting on curved substrates, Phys. Rev. Mater. 2 (2018) 113401.
[32] W. Jiang, Q. Zhao, Sharp-interface approach for simulating solid-state dewetting in two dimensions: a Cahn-Hoffman ξ-vector formulation, Physica D 390 (2019) 69–83.
[33] W. Jiang, Q. Zhao, W. Bao, Sharp-interface model for simulating solid-state dewetting in three dimensions, SIAM J. Appl. Math. 80 (2020) 1654–1677.
[34] W. Jiang, B. Li, A perimeter-decreasing and area-conserving algorithm for surface diffusion flow of curves, J. Comput. Phys. 443 (2021) 110531.
[35] M. Li, Y. Li, L. Pei, A symmetrized parametric finite element method for simulating solid-state dewetting problems, Appl. Math. Model. 121 (2023) 731–750.
[36] Y. Li, W. Bao, An energy-stable parametric finite element method for anisotropic surface diffusion, J. Comput. Phys. 446 (2021) 110658.
[37] C. Mantegazza, Lecture Notes on Mean Curvature Flow, Springer Science & Business Media, 2011.
[38] W. Mullins, Theory of thermal grooving, J. Appl. Phys. 28 (1957) 333–339.
[39] K. Oura, V. Lifshits, A. Saranin, A.Zotov, M. Katayama, Surface Science: an Introduction, Springer Science & Business Media, 2013.
[40] S. Randolph, J. Fowlkes, A. Melechko, K. Klein, H. Meyer, M. Simpson, P. Rack, Controlling thin film structure for the dewetting of catalyst nanoparticle arrays for subsequent carbon nanofiber growth, Nanotechnology 18 (2007) 465304.
[41] O. Reynolds, Papers on Mechanical and Physical Subjects, CUP Arch, 1983.
[42] H. Shen, S. Nutt, D. Hull, Direct observation and measurement of fiber architecture in short fiber-polymer composite foam through micro-CT imaging, Compos. Sci. Technol. 64 (2004) 2113–2120.
[43] E. Shustorovich, Metal-Surface Reaction Energetics. Theory and Application to Heterogeneous Catalysis, Chemisorption, and Surface Diffusion, VCH Publ. Inc., New York, 1991.
[44] D. Srolovitz, S. Safran, Capillary instabilities in thin films. II. Kinetics, J. Appl. Phys. 60 (1986) 255–260.
[45] T. Tang, Z. Qiao, Efficient numerical methods for phase-field equations (in Chinese), Sci. China Ser. A 50 (2020) 1–20 (in Chinese).
[46] J. Taylor, II-mean curvature and weighted mean curvature, Acta Metall. Mater. 40 (1992) 1475–1485.
[47] J. Taylor, J. Cahn, Linking anisotropic sharp and diffuse surface motion laws via gradient flows, J. Stat. Phys. 77 (1994) 183–197.
[48] C. Thompson, Solid-state dewetting of thin films, Annu. Rev. Mater. Res. 42 (2012) 399–434.
[49] Y. Wang, W. Jiang, W. Bao, D. Srolovitz, Sharp interface model for solid-state dewetting problems with weakly anisotropic surface energies, Phys. Rev. B 91 (2015) 045303.
[50] H. Wong, P. Voorhees, M. Miksis, S. Davis, Periodic mass shedding of a retracting solid film step, Acta Mater. 48 (2000) 1719–1728.
[51] Y. Xu, C. Shu, Local discontinuous Galerkin method for surface diffusion and Willmore flow of graphs, J. Sci. Comput. 40 (2009) 375–390.
[52] J. Ye, C. Thompson, Mechanisms of complex morphological evolution during solid-state dewetting of single-crystal nickel thin films, Appl. Phys. Lett. 97 (2010).
[53] Q. Zhao, W. Jiang, W. Bao, An energy-stable parametric finite element method for simulating solid-state dewetting, IMA J. Numer. Anal. 41 (2021) 2026–2055.